
**Study of the Track Reconstruction Efficiency
Exploiting Partially Reconstructed Decays
at the LHCb Experiment**

Sarah Lindner

Karl-Franzens University of Graz

Diploma thesis

Supervisor:

Prof. Dr. Stephanie Hansmann-Menzemer
Physikalisches Institut, University of Heidelberg

March 2013

Abstract

A novel method to derive track reconstruction efficiencies for the LHCb spectrometer is presented. This purely data-driven method especially focuses on taking potential effects of material interaction into account. It is based on a tag-and-probe approach using partially reconstructed $B^+ \rightarrow J/\Psi(\mu\mu)K^+$ and $\Lambda \rightarrow p\pi^-$ decays. The method is first validated on Monte Carlo and then applied to data taken by the LHCb experiment. Statistical uncertainties on the track finding efficiency of 2.5% and 0.07% for the study of B^+ and Λ decays are obtained, respectively.

Contents

Table of Contents	i
List of Figures	ii
List of Tables	iv
Acknowledgements	v
1 Introduction	1
2 The Large Hadron Collider Beauty Experiment	2
2.1 The LHCb detector	3
2.1.1 Vertex Locator	4
2.1.2 Tracking Stations	6
2.1.3 Ring Imaging Cherenkov Detectors	8
2.1.4 Calorimeters	8
2.1.5 Muon System	9
2.2 Trigger	9
2.3 Physics at LHCb	11
3 Track Reconstruction at LHCb	14
3.1 Track Types	15
3.2 Algorithms	16
3.2.1 Reconstruction of Vertex Locator Tracks	16
3.2.2 Reconstruction of Long Tracks	17
3.3 Software	17
3.4 Efficiency	18
4 Measurement of the Tracking Efficiency on Data Using the Decay Channel $B^+ \rightarrow J/\psi K^+$	20
4.1 Introduction	20
4.2 Efficiency Using Tag-And-Probe	22
4.3 Reconstruction Method	23
4.4 Event Selection	25
4.4.1 Custom-Made Cuts	25
4.4.2 Standard Cuts	29
4.5 B^+ Mass Distribution	31
4.5.1 Monte Carlo $B^+ \rightarrow J/\psi K^+$ Sample	31

4.5.2	Monte Carlo J/Ψ inclusive Sample	31
4.5.3	Data Sample	33
4.6	Efficiency Calculation	36
4.6.1	Long Track Matching	36
4.6.2	Signal - Background Separation	36
4.7	Results	40
4.8	Discussion	43
4.8.1	Error Calculation	43
4.8.2	Comparison Monte Carlo- Data	43
4.8.3	Factors Reducing the Efficiency	43
4.8.4	Conclusion	44
5	Measurement of the Tracking Efficiency on Data Using the Decay Channel	
	$\Lambda \rightarrow p\pi^-$	46
5.1	Introduction	46
5.2	Reconstruction Method	48
5.3	Event Selection	49
5.3.1	Candidate Selection Cuts	49
5.3.2	Cuts to Enhance Reconstruction Probability	50
5.4	Λ Mass Distribution	51
5.4.1	Monte Carlo $\Lambda \rightarrow p\pi^-$ Sample	51
5.4.2	Data Sample	52
5.5	Efficiency Calculation	54
5.5.1	Signal - Background Separation	54
5.6	Results, Discussion	57
5.6.1	Outlook	59
6	Conclusion	60
A	Fit Parameters	61
A.1	$B^+ \rightarrow J/\Psi K^+$	61
A.2	$\Lambda \rightarrow p\pi^-$	63
B	Derivation of Kaon Momentum	65
	Bibliography	67
	Index	69

List of Figures

2.1	LHC sketch	3
2.2	LHCb detector	4
2.3	Angles of a $b\bar{b}$ event.	5
2.4	Vertex Locator	5
2.5	LHCb Tracker	6
2.6	LHCb Outer Tracker, Straw Tubes	7
2.7	LHCb Cherenkov Detector	7
2.8	LHCb Calorimeter Sketch	8
2.9	Trigger	10
2.10	Standard Model of Particle Physics	11
2.11	Flavor Changing Neutral Currents [1].	13
3.1	State Vector of a Track	14
3.2	LHCb event display	15
3.3	Track Types	16
3.4	Forward tracking	17
3.5	Workflow of the reconstruction software	18
4.1	$B^+ \rightarrow J/\Psi K^+$ decay	21
4.2	$B^+ \rightarrow J/\Psi (\mu\mu) K^+$ decay in LHCb detector	21
4.3	$B^+ \rightarrow J/\Psi K^+$ decay - VELO stub in detector	23
4.4	Momenta of the $B^+ \rightarrow J/\Psi K^+$ decay	24
4.5	Histogram track-vertex-distance	26
4.6	Histogram clone angle	27
4.7	Isolation cut	28
4.8	Isolation cut histogram	28
4.9	Cosine of the maximized angle	29
4.10	Impact parameter	30
4.11	Monte Carlo B^+ mass, before final cuts.	32
4.12	Monte Carlo B^+ mass, $B^+ \rightarrow J/\Psi K^+$ sample, after final cuts.	32
4.13	Monte Carlo B^+ mass, J/Ψ inclusive sample, after cuts.	33
4.14	$B^+ \rightarrow J/\Psi K^+$ events vs. $B^+ \rightarrow J/\Psi K^{*+}$ events	34
4.15	B^+ mass, data sample	35
4.16	Monte Carlo background fit; in detector acceptance	37
4.17	Monte Carlo fit divided into background and signal; fit goodness	39
4.18	Fit of the invariant mass of the B^+ particle of partially reconstructed $B^+ \rightarrow J/\Psi K^+$ candidates obtained with simulated data.	41

4.19	Fit of the invariant mass of the B^+ particle of partially reconstructed $B^+ \rightarrow J/\Psi K^+$ candidates obtained with simulated data.	41
4.20	Fit of the invariant mass of the B^+ particle of partially reconstructed $B^+ \rightarrow J/\Psi K^+$ candidates obtained with data taken by LHCb.	41
4.21	Amount of kaon decays in detector modules.	45
5.1	$B^+ \rightarrow J/\Psi K^+$ decay	47
5.2	$\Lambda \rightarrow p\pi^-$ decay - VELO stub in detector	48
5.3	Selection cuts on Monte Carlo $\Lambda \rightarrow p\pi^-$ sample	51
5.4	Λ mass peak, Monte Carlo truth matched.	52
5.5	Λ mass distribution, data	53
5.6	Fit goodness Monte Carlo $\Lambda \rightarrow p\pi^-$	55
5.7	Fit LHCb data $\Lambda \rightarrow p\pi^-$	56
5.8	Fit of the Λ mass obtained with simulated data.	58
5.9	Fit of the Λ mass obtained with simulated data.	58
5.10	Fit of the Λ mass obtained with data taken in LHCb.	58

List of Tables

4.1	Cuts applied to $B^+ \rightarrow J/\Psi K^+$ samples.	30
4.2	Amount of particle decays listed by the detector part and in which they decay. T1,T2 and T3 refer to the three tracking modules after the magnet.	44
5.1	Cuts applied to $\Lambda \rightarrow p\pi^-$ samples.	50
A.1	Fitting parameters for the background function. $\chi^2 = 43.8384$	61
A.2	Monte Carlo in acceptance $\chi^2 = 35.6567$	61
A.3	Monte Carlo not in acceptance $\chi^2 = 54.9194$	61
A.4	Monte Carlo long tracks matched. $\chi^2 = 82.073$	62
A.5	Monte Carlo long tracks not matched. $\chi^2 = 47.6703$	62
A.6	Data long tracks matched. $\chi^2 = 48.676$	62
A.7	Data long tracks not matched. $\chi^2 = 28.7613$	62
A.8	Monte Carlo in acceptance. $\chi^2 = 53.461$	63
A.9	Monte Carlo not in acceptance. $\chi^2 = 42.6651$	63
A.10	Monte Carlo long tracks matched. $\chi^2 = 181.89$	63
A.11	Monte Carlo long tracks not matched. $\chi^2 = 395.548$	64
A.12	Data long tracks matched. $\chi^2 = 1012.24$	64
A.13	Data long tracks not matched. $\chi^2 = 459.96$	64

Acknowledgements

First of all, I want to thank my supervisor, Prof. Dr. Stephanie Hansmann-Menzemer, for the opportunity of writing my diploma thesis in a group performing research on the topic of experimental particle physics. I owe her my utmost gratitude, because several complications arose due to the fact, that writing the diploma thesis at a university abroad is not the regular way foreseen by study regulations. I am especially thankful for her guidance during my work on this diploma thesis.

I am very grateful for the guiding help of Sebastian Wandernoth, who never tired of answering my questions. I want to express my special thanks to my office colleagues Katharina Kreplin and Georg Krockner for the nice working environment. I also want to thank the whole LHCb group at Heidelberg for their support.

I am grateful to all the professors, lecturers and teaching assistants at the University of Graz for providing an excellent physics education, especially Ao. Univ.-Prof. Dr. Willibald Plessas, Univ.-Prof. Dr. Franz Aussenegg, Univ.-Prof. Dr. Joachim Krenn and Dr. Dipl. Ing. Andreas Hohenau, who all had a big impact on my understanding of physics.

I owe special thanks to Daniela Gaar, who solved seemingly unresolvable bureaucratic and organizational problems.

With all the friends I found during my studies in Graz, even times of excessive studying became agreeable. Special thanks go to Veronika Schweinzer and Michael Dirnberger for their moral support.

Finally I want to thank my family for their support during my studies. In particular, I want to thank my mum who taught me the importance of knowledge and my dad who introduced me to the great fascination of physics.

Chapter 1

Introduction

The LHCb experiment is one of the four major experiments at the Large Hadron Collider at CERN. It aims at searching New Physics phenomena beyond the Standard Model of particle physics. The Standard Model describes results of collider experiments extremely well, no significant deviation has been found up to now. However, nature poses some questions which cannot be answered within this model. For example, one unexplained observation is that matter dominates anti-matter in the universe, even though they were created in same amounts after the Big Bang. The particle-antiparticle asymmetry introduced in the Standard Model is by far too small to explain the observed effects in the universe.

The objective of LHCb is the indirect search for New Physics phenomena using high precision measurements of quantum loop induced effects. For this purpose, heavy hadron decays containing a beauty or charm quark are examined. New Physics would manifest itself as small corrections to Standard Model processes. To perform these high precision measurements it is crucial to understand possible sources of uncertainties in detail. At the moment, the largest source of systematic uncertainties of many LHCb measurements is the uncertainty of the track reconstruction efficiency. Especially uncertainties of the possible difference between positively and negatively charged tracks contribute. They are caused by different material interaction properties. So far, the track reconstruction efficiency has been evaluated in LHCb considering particles which traversed the whole detector [2]. The aim of this thesis is to explicitly include effects of material interaction.

Therefore a tag-and-probe method is developed using partially reconstructed decays to calculate the track reconstruction efficiency. This method only requires that the probe particles pass through the first sub-detector. Thus it is sensitive to material effects in the later tracking detectors.

In chapter 2 an introduction to the LHCb experiment is given. In the following chapter, the track reconstruction of charged particles at LHCb is summarized. The tag-and-probe method using partially reconstructed decays for determining the track reconstruction efficiency is described in chapter 4 and chapter 5, using the $B^+ \rightarrow J/\Psi K^+$ and $\Lambda \rightarrow p \pi^-$ decays respectively. Finally chapter 6 summarizes the results of this work.

Chapter 2

The Large Hadron Collider Beauty Experiment

The Large Hadron Collider (*LHC*) is a particle collider which is situated near Geneva, Switzerland and lies about 100 m below ground level. It is one of the ongoing projects at the European Organization for Nuclear Research, CERN (French: Conseil Européenne pour la Recherche Nucléaire).

The purpose of LHC is to collide either protons or heavy ions. It was designed for a center of mass energy \sqrt{s} of 14 TeV for proton-proton collisions; at the time of performing the work for this thesis it is running at $\sqrt{s} = 7$ TeV.

The protons are subsequently accelerated in one linear and two circular accelerators, then fed into the 27 km circumference LHC ring in bunches of approximately 10^{11} protons. There are two proton beams moving into opposite directions. For each beam there is a separate beam pipe. The beam pipes cross at four points allowing the particle bunches to collide, which at this time happens once every 50 ns. At these crossing points the detectors are located (fig. 2.1).

The four major experiments at LHC are called ALICE (A Large Ion Collider Experiment), ATLAS (A Toroidal LHC ApparatuS), CMS (Compact Muon Solenoid) and LHCb (LHC Beauty experiment).

The ALICE experiment focuses on the study of quark-gluon plasma and strongly interacting matter in heavy ion collisions. ATLAS and CMS are multi-purpose detectors built for the search of new heavy particles which are produced at high energies. Their goal is to detect their decay products and therefore find evidence of New Physics. This approach is called direct search.

LHCb is carrying out measurements at high precision with a special focus on particles containing a beauty-quark (so-called *B-Physics*). The aim of these precision experiments is the indirect search for New Physics. New Physics would manifest itself as corrections to specific physical processes described by the Standard Model of particle physics, namely quantum loop corrections (section 2.3). With the method pursued at LHCb, it is possible to find indications of New Physics at higher energy scales than ATLAS or CMS.

For further information on ALICE, ATLAS and CMS, see [3], [4] and [5], respectively.

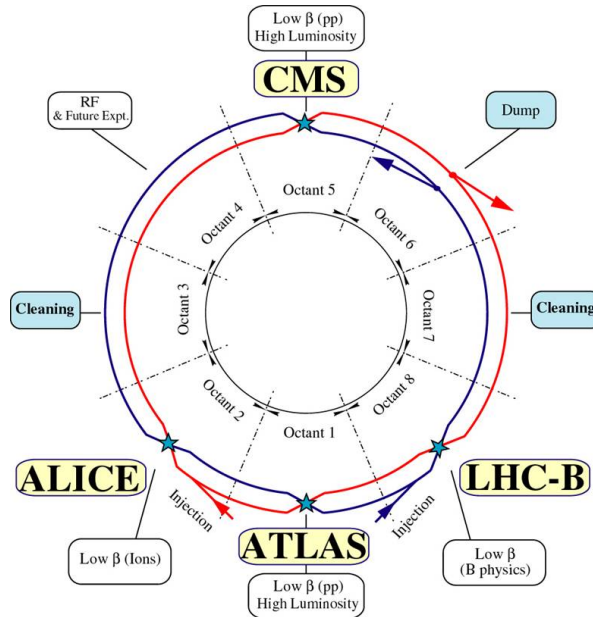


Figure 2.1: Sketch of the LHC ring, indicating the location of the four major experiments. The red circle shows the beam pipe with particles traveling in one direction, in the beam pipe indicated in blue, particles move in the opposite direction [6].

2.1 The LHCb detector

The *LHCb* detector [7] is a forward spectrometer (fig. 2.2). This architecture was chosen because b and \bar{b} particles are mainly produced in a cone around the beam axis (fig. 2.3). They are produced in same amounts in the forward and the backward region, however one direction was chosen.

In particle physics, the quantity *pseudorapidity* η is often used to express the detector acceptance. It is a dimensionless redefinition of the angle with respect to the beam axis in the middle of the detector. With the angle being denoted as Θ , the pseudorapidity is defined as:

$$\eta = -\ln \left(\tan \left[\frac{\Theta}{2} \right] \right) \quad (2.1)$$

Therefore $\eta = \infty$ at the beam axis and 0 perpendicular to the beam axis. The sector of possible detection of particles, called detector acceptance is $1.6 < \eta < 4.9$. The lower limit is caused by the beam pipe, the upper limit by the outer border of the detector parts.

The detector is designed for an *instantaneous luminosity* of $2 \times 10^{32} \text{ cm}^{-2}\text{s}^{-1}$. It corresponds to the number of collisions per unit area per time: $L = fn \frac{N_1 N_2}{A}$, where f denotes the revolution frequency, n the number of bunches per beam, N_i the number of particles per bunch, and A the cross section of the beam. With the given luminosity, about 10^{12} $b\bar{b}$ pairs are produced in one nominal year of data taking.

The following sub-detectors form the detector: the *Vertex Locator* (short VELO), the *tracking stations* (TT, T1-T3), two *Ring Imaging Cherenkov Detectors* (RICH1, RICH2), an *electromagnetic calorimeter* (ECAL), a *hadronic calorimeter* (HCAL), and a *muon identification system* (M1-M5) (sections 2.1.1 to 2.1.5). The magnet to bends the trajectories of charged particles which is necessary to determine the particles' momenta.

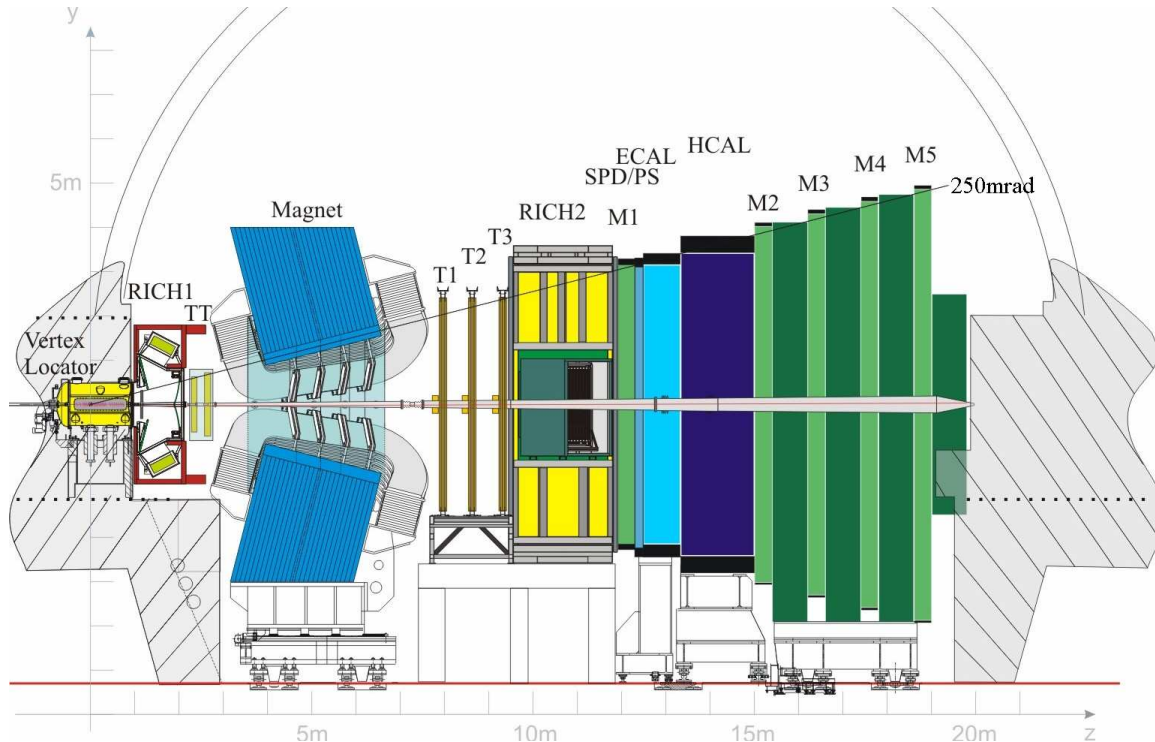


Figure 2.2: Sketch of the LHCb detector, side view [7].

The used convention for the coordinate system is a left-handed coordinate system with the x coordinate pointing to the center of the collider ring, therefore y corresponds to the height and z coincides with the beam axis. The origin is situated at the proton-proton interaction point.

To make a first distinction between signal and background, a trigger decides, whether an event should be recorded (section 2.2).

2.1.1 Vertex Locator

The *Vertex Locator* [9] (fig. 2.4) is a silicon strip detector, aimed at precisely locating the primary and secondary vertices. It is composed up of 2 times 21 half-discs on either side of the beam in a vessel maintaining beam vacuum. The half discs comprise either a radial or a circular silicon strip structure, in alternating order. The reason for the alternating design is the following: In the half disk with radial structure (Φ sensors), the angle on the plane orthogonal to the beam axis is detected. In the following disc with circular strip structure (r sensors), the radius with respect to the beam pipe is measured. The spatial resolution of the primary vertex in the Vertex Locator is $42 \mu\text{m}$ in the beam direction and $10 \mu\text{m}$ perpendicular to the beam [10].

The major advantage of the LHCb Vertex Locator is, the possibility of varying the spacing between the opposite half discs. During beam setup and beam dumping, the spacing is put to the “open” state (fig. 2.4), to avoid damaging of the detector. Once the beam is stable, the half discs are closed, allowing them to detect particles at a distance of only 8 mm from the beam.

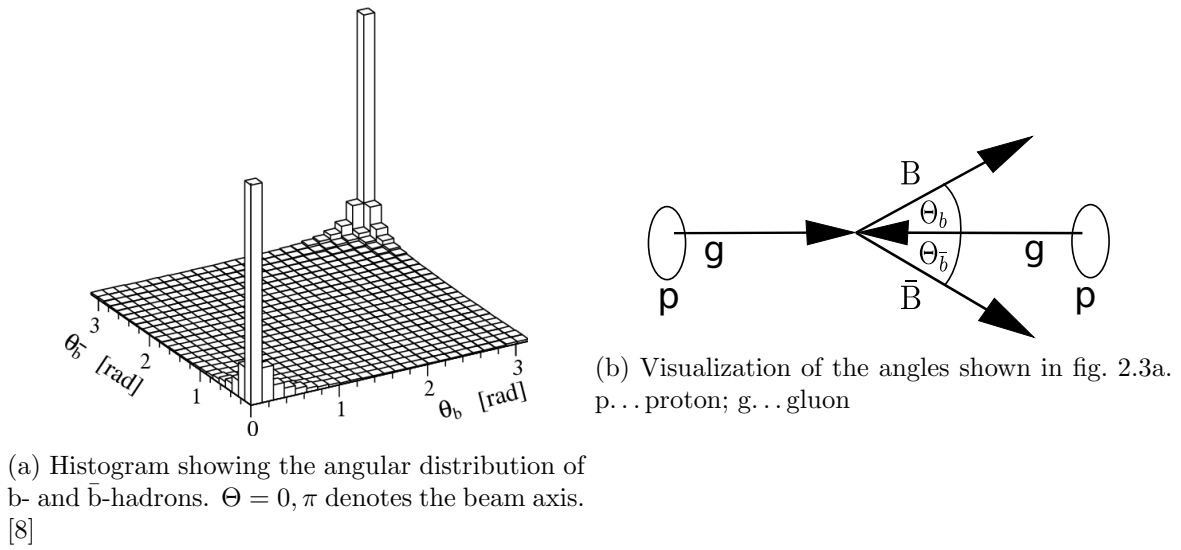


Figure 2.3: Angles of a $b\bar{b}$ event.

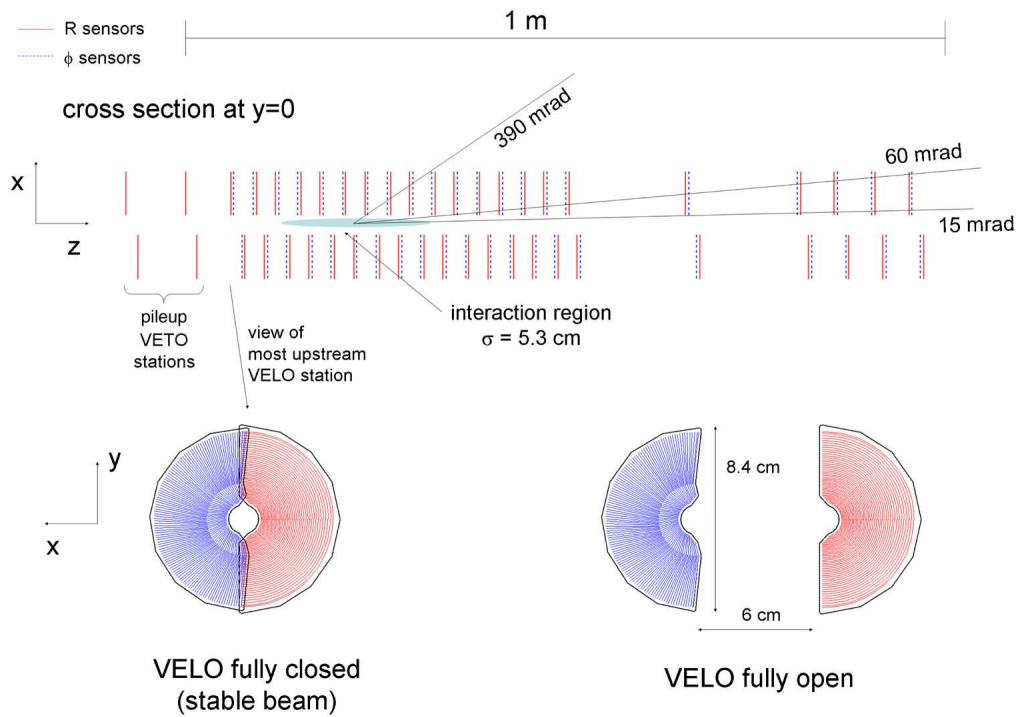


Figure 2.4: Top: Setup of the Vertex Locator. The lower boundary of the acceptance (15 mrad) and the upper boundary (390 mrad) are indicated for the requirement of at least 3 crossings of a trajectory with Vertex Locator modules. Bottom: Sketch of the Vertex Locator discs with the radial and the circular structures. The open and the closed states are shown [7].

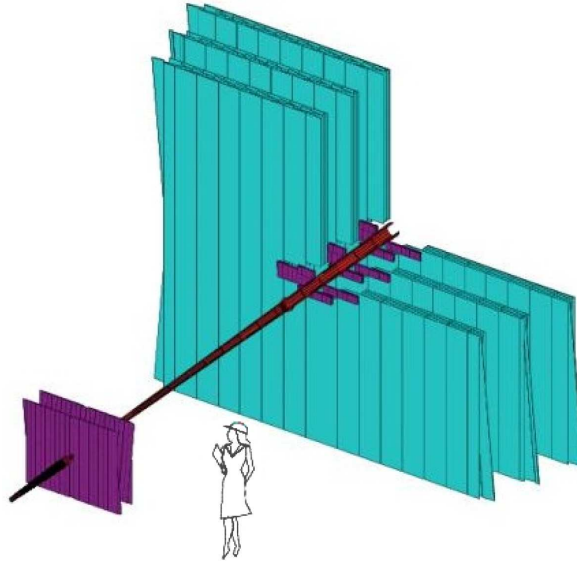


Figure 2.5: Sketch of the Tracking Stations with the beam pipe passing through in the middle. The two planes at the left-hand side indicate the Trigger Tracker, the cross-shaped purple parts close to the beam pipe at the right-hand side indicate the Inner Tracker components. The big blue planes at the right-hand side illustrate the Outer Tracker modules [7].

2.1.2 Tracking Stations

The tracking stations consist of the *Trigger Tracker* [7] (abbreviated *TT*) in front of the magnet and three tracking stations after the magnet (T1-T3 in fig. 2.2; fig. 2.5). The purpose of the tracking stations is to detect the trajectories of charged particles. This process is called *tracking*.

The main purpose of the Trigger Tracker is to collect information for the trigger decisions, as the name suggests (section 2.2). It also serves to enhance momentum measurements.

The tracking modules after the magnet are each again divided into Inner Tracker and Outer Tracker. The Inner Tracker covers the area close to the beam pipe where the particle flux is highest, the Outer Tracker is built around the Inner Tracker part to cover the area at a greater distance to the beam pipe.

Trigger Tracker and Inner Tracker

Both the Trigger Tracker and the Inner Tracker are silicon strip detectors: If a charged particle passes through the silicon, it causes ionization. An external electric field induces a drift of the free electrons and holes, which is measured as a current.

The strip architecture provides only one dimensional information. To gain access to the other two dimensions, each of the Inner Tracker and the Trigger Tracker detector modules consists of four layers: While in the first and the fourth layer the strips are arranged vertically, the orientations in the second and the third layer are inclined at an angle of -5° and $+5^\circ$, respectively. The point where a particle traverses is given by the crossing point of strips in consecutive layers detecting a signal.

The active area of the Trigger Tracker is 8.4 m^2 , of the Inner Tracker it is 4 m^2 . The spatial resolution of both the Trigger Tracker and the Inner Tracker is about $50 \mu\text{m}$ [7]. Momentum resolution of a particle is then dominated by multiple scattering, which is the process of a

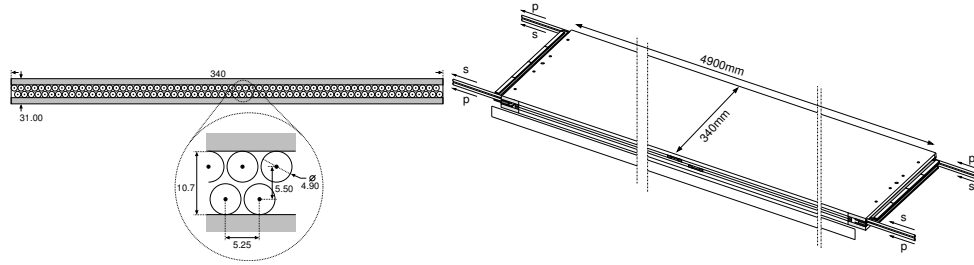


Figure 2.6: Partial view of an Outer Tracker module with its two monolayers of straw tubes [7].

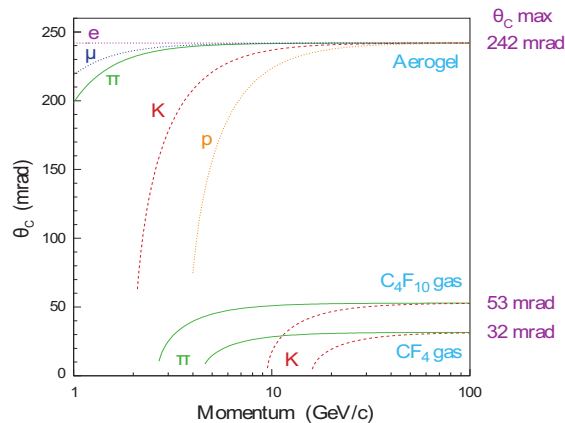


Figure 2.7: Cherenkov angle of different particles vs. momentum in the materials used by the LHCb ring imaging cherenkov detectors. It can be seen, that in one medium, every particle has a very distinct line. [7]

particle being scattered several times along its path, each time losing energy. Hence, the more a particle scatters, the worse is the momentum resolution.

Outer Tracker

Opposed to the TT and the Inner Tracker, the Outer Tracker is a drift-time detector. This provides tracking of charged particles and the measurement of their momenta over a large acceptance area [7]. The Outer Tracker is built using the same four-layer architecture as the Trigger Tracker and the Inner Tracker. Each layer is composed of two monolayers of straw tubes (fig. 2.6) which are filled with Argon and CO_2 . In the middle of each tube, there is an anode wire. A particle traversing a tube ionizes the gas, causing free electrons and ions, which drift towards the anode and the cathode, respectively. Due to the accumulation of electrons at the anode wire and ions at the cathode tube a current can be measured. The Argon and CO_2 realize a short drift time of below 50 ns.

The Outer Tracker's upper limit of the angle of particle detection is 300 mrad in the horizontal plane and 250 mrad in the vertical plane. As the magnet bends particle trajectories in the horizontal plane, a bigger horizontal angular acceptance is advantageous. The spatial resolution is about 200 μm .

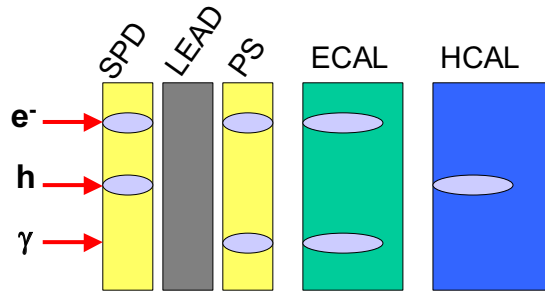


Figure 2.8: Sketch of the Calorimeter System. It is indicated, where an electron (e^-), a hadron (h) and a photon (γ) would leave signals [11].

2.1.3 Ring Imaging Cherenkov Detectors

If the velocity of a charged particle moving in a dielectric medium is higher than the speed of light in that medium, it emits light called *Cherenkov radiation*. It is emitted in a cone around the moving particle, with an opening angle of

$$\tan \Theta_C = \frac{1}{n\beta} \quad (2.2)$$

where n denotes the refractive index of the medium and $\beta = v/c$ is the ratio between the speed of the particle and the speed of light in vacuum.

Within the two *Ring Imaging Cherenkov Detectors* at LHCb (short: RICH1 and 2) each Cherenkov photon passes through an optical system and is then detected by Hybrid Photon Detectors. These photon detectors make an image of the rings due to the Cherenkov light cone shape. Thus the angle Θ_C at the emission point can be traced back. In fig. 2.7 the Cherenkov angles for different particles in the media used by both RICH detectors are shown.

RICH1 is filled with aerogel and fluorobutane (C_4F_{10}), *RICH2* with CF_4 gas. The refractive indices of these materials are known, therefore the particle's velocity can be calculated using eq. (2.2). As the momentum is measured by the Tracking Stations, the particle's mass can be calculated via the equation for the relativistic momentum:

$$p = mv\gamma = \frac{mv}{\sqrt{1 - \frac{v^2}{c^2}}} \quad (2.3)$$

The mass gives indication of the particle type in question.

At LHCb the Cherenkov detectors were primarily designed to distinguish pions, kaons and protons. RICH1 covers the low momentum range, RICH2 the high momentum range. A clear distinction between kaons and pions is crucial for *B-Physics*, as they appear in various B decay modes. For several interesting decay channels, the difference between an event being signal or background is determined by the decay products being kaons or pions.

2.1.4 Calorimeters

The calorimeters' tasks are twofold. Firstly, they distinguish photons, electrons and hadrons and measure their energies and positions. Secondly, they pass information of transverse energy to the hardware *trigger*. The *trigger* decides whether or not an event should be recorded (section 2.2).

The LHCb calorimeter system comprises the following: a *Scintillator Pad Detector / PreShower Detector (SPD/PS)*, followed by an electromagnetic calorimeter, which is followed by a HCAL. The Scintillator Pad Detector identifies charged particles, and allows distinguishing electrons from photons [11]. The PreShower Detector contributes to identifying electrons and photons [12]. While electrons are fully stopped in the electromagnetic calorimeter (entire radiation length $25 X_0$), hadrons pass until their whole energy is absorbed in the hadronic calorimeter (fig. 2.8). The hadronic calorimeter has a length of 5.6 hadronic interaction lengths λ_I .

Both the electromagnetic calorimeter and the hadronic calorimeter work according to the same principle: They consist of alternating layers of absorber material and scintillators. The absorber material of the electromagnetic calorimeter is lead, the hadronic calorimeter's absorber is iron. In the scintillators light is produced, which is then collected and recorded. The energy of a particle corresponds to the number of photons detected.

The energy resolutions are approximately [13]:

$$\text{electromagnetic calorimeter} \quad \frac{\sigma(E)}{E} = \frac{10\%}{\sqrt{E/\text{GeV}}} \oplus 1\% \quad (2.4)$$

$$\text{hadronic calorimeter} \quad \frac{\sigma(E)}{E} = \frac{80\%}{\sqrt{E/\text{GeV}}} \oplus 11\% \quad (2.5)$$

2.1.5 Muon System

Events with muons as decay products are particularly interesting in particle physics, because they leave a clear signal in the detector. The tasks of the *Muon System* are identifying events containing muons and measuring the muons' momenta.

As already mentioned, the trigger decides if an event is recorded or rejected. Information about whether or not an event contains muons is part of the information needed for certain trigger decisions.

Muons are the only particles passing through the calorimeters (except neutrinos), all the other particles produced in the collision are absorbed in the calorimeter material. Hence by building the Muon System after the calorimeters, the muons are separated from background by the setup of the detector.

The *Muon System* (M1-M5 in fig. 2.2) consists of five separate modules, which are called stations. The *Muon Stations* are multi wire proportional chambers. In these gas filled chambers, planes of high voltage wires and planes of so-called sense wires at ground level alternate. The method of operation is similar to straw tube detectors: A charged particle passes through the detector, ionizing gas. The thereby freed electrons move towards the sense wire, causing an electric signal.

2.2 Trigger

A crucial ingredient to reconstruct the full B decay is having a low number of primary interactions per event. Therefore the high achievable luminosity of LHC is reduced. A fortunate side effect of a lower luminosity is the fact that it causes less radiation damage to the detector. The initial crossing frequency with detectable interactions has to be reduced from 40 MHz to 2 kHz. At the final rate, data recording is possible [7],[14].

The selection of events is performed exploiting the following aspects:

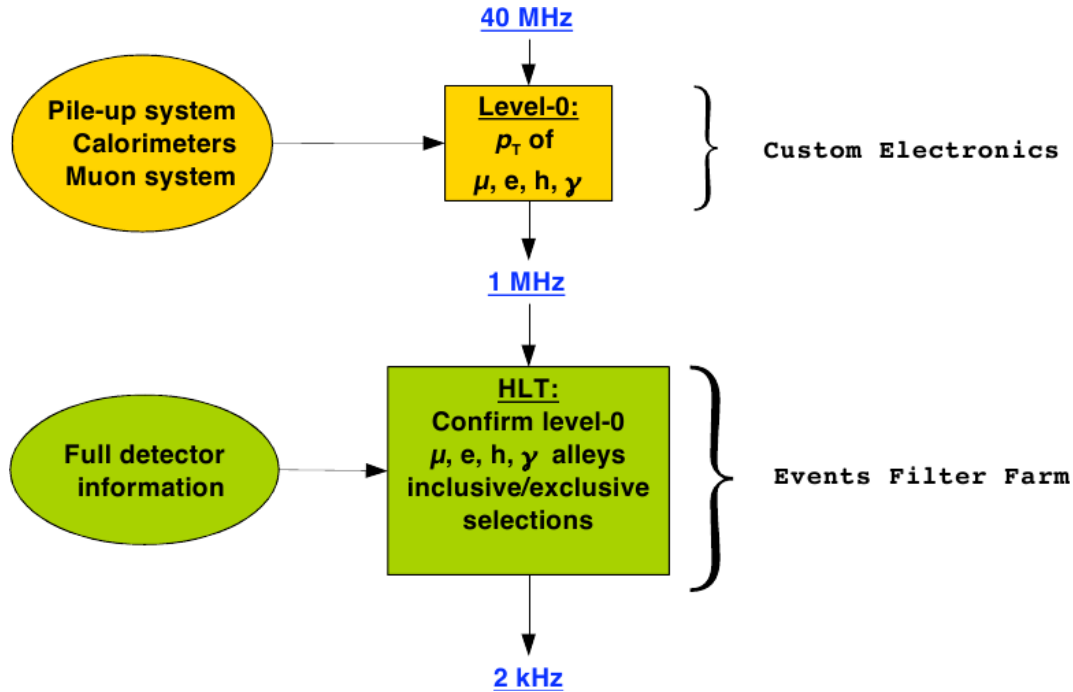


Figure 2.9: Workflow of the LHCb trigger [7].

- B-meson properties
 - B lifetime, determined by displacement of the vertices
 - B mass, manifests itself via transverse energy E_t and transverse momentum p_t of the decay products
- cleanest B events
 - Veto events with more than one collision (no pile-up)
 - Veto events with too high track multiplicity

The trigger is divided into an electronic hardware trigger (Level-0 trigger) and a software trigger (*High Level Trigger*, HLT) running on more than 15000 processors, called Event Filter Farm (fig. 2.9).

The hardware trigger uses mainly information from the calorimeters and the muon system. The VELO trigger is only needed for decisions due to pile-up. At the time when the Level-0 trigger decides to keep an event, the event is not reconstructed. The only input information to the trigger are interaction points and the deposited energies in the calorimeters. Due to their large mass, decays of B mesons often produce particles with large transverse momenta and energies. Therefore the Level-0 trigger focuses on reconstructing events with highest transverse energy of hadrons, electrons and photons measured by the calorimeters and the highest transverse momentum muons in the muon chambers. Furthermore, events with multiple collisions are vetoed by the Vertex Locator and by the Scintillator Pad Detector of the calorimeters, also events with too many tracks are filtered out. The time elapsing from collision to hardware trigger decision is $4 \mu\text{s}$.

The software trigger partially reconstructs decays, which can be done faster than a full reconstruction. An advantage is, the possibility of adjusting the software if other trigger

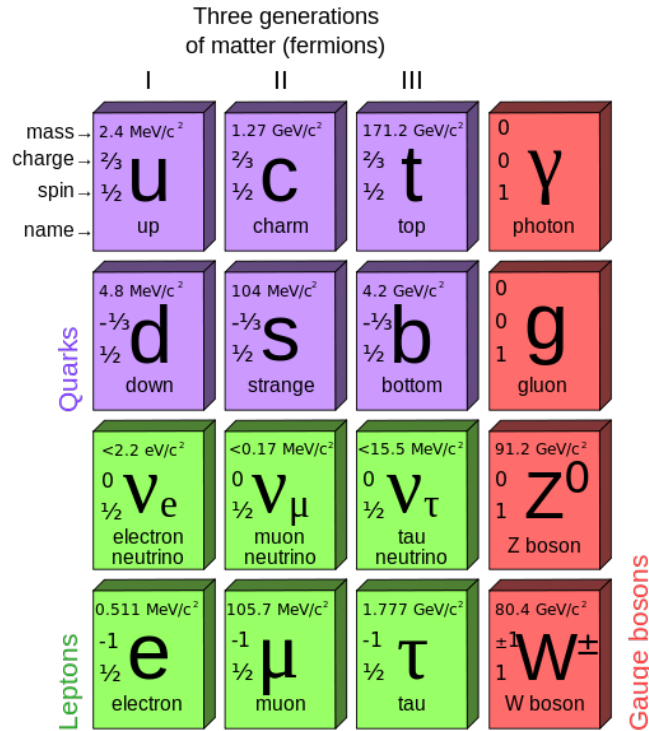


Figure 2.10: Elementary Particles comprised by the Standard Model of Particle Physics [16].

requirements should be desired. The High Level Trigger has access to full event data. It is divided into HLT1 and HLT2. HLT1 partially reconstructs tracks, identifies leptons and applies cuts to reduce the crossing frequency. HLT2 reconstructs all events with a transverse momentum higher than 500 MeV. The input used for the HLT2 trigger decision are leptonic decays, finite lifetime and invariant mass [15].

2.3 Physics at LHCb

The theory uniting the well-established knowledge of particle physics is the *Standard Model* of particle physics, which describes experimental results to a high accuracy. It states that matter consists of a limited number of elementary particles and that interactions are mediated by particles. These particles are divided into fermions having half-integer spin and gauge bosons having integer spins (fig. 2.10). The fermions are the building blocks of matter. They are divided into two different types: quarks and leptons. If two fermions interact, they do so by exchanging a gauge boson. The photon is the force carrier of the electromagnetic interaction, the gluon is the force carrier of the strong interaction and the Z and W bosons are the force carriers of the weak interaction.

To every particle there exists a partner with opposite internal quantum numbers (charge, lepton number...), called its *antiparticle*. The bosons without charge are their own antiparticles.

Quarks form bound states, called hadrons. There are two types of hadrons: Mesons which consist of one quark and one antiquark and Baryons which consist of either three quarks or three antiquarks. The most popular types of baryons are the neutron and the proton.

Together with the electron they form atoms.

The Big Bang produced particles and antiparticles in the same amount. If a particle meets its antiparticle partner, they annihilate. Yet at present-day there are only particles left, therefore, matter has been dominating over antimatter. Processes which could explain this inequality are summarized by the term baryogenesis. For example, one explanation is that particles and antiparticles have different decay rates. Today, the different decay rates of a particle and its antiparticle are described by *CP violation* (Charge-Parity violation) in weak interactions, which is the breaking of the Charge-Parity-Symmetry. CP-symmetric processes are invariant under the interchanging of particles and antiparticles (Charge symmetry) and the inversion of the three spatial coordinate axes (Parity symmetry). CP is conserved in most interactions, but violated in some weak processes. It is these rare processes which are particularly interesting to investigate, as they could give answers to the question why there is such a big dominance of matter over antimatter in the universe. The amount of CP violation needed to explain the present matter dominated universe cannot be explained within the Standard Model, therefore New Physics theories beyond the Standard Model are needed [17].

LHCb performs indirect searches for New Physics phenomena, accessible via quantum corrections to the Standard Model processes. Indirect search is performed with experiments which do not aim at directly producing new particles and measuring their decay products, but rather at finding the effects such particles would have on known physics processes. To probe these processes, measurements with high precision are crucial. Observables, which are not yet investigated to the last detail are measured. If these deviate from the values expected by Standard Model calculations, a hint for New Physics is found.

There are two different approaches pursued by LHCb to detect New Physics phenomena [18]: The first one is to probe CP-asymmetries in CP violating decays. The amount of CP violation in the Standard Model is very small, New Physics manifests itself as contributions to the Standard Model processes. One of these processes is called mixing: The eigenstates of the weak interaction and the mass eigenstates are not the same. This causes neutral mesons (e.g. B^0) to turn into their antimatter partner and vice versa. Measuring the frequency of the oscillation between particle and antiparticle provides insight to possible contributions from New Physics.

Another approach is to study branching ratios which are very small in the Standard Model. The branching ratio describes the probability of a particle decaying in a particular decay channel with respect to all possible decay channels. If these small branching ratios are found to be bigger than expected, New Physics theories would be needed as explanation. The therefore required analysis is carried out laying emphasis on Flavor Changing Neutral Currents (FCNC): Flavor change means the change from one quark type (flavor) into another. In flavor changing weak interactions, the neutral current requires the exchange of the neutral Z boson. In the Standard Model, Flavor Changing Neutral Currents are suppressed in first order, but they are allowed in second order corrections (fig. 2.11). These are quantum loop corrections and occur in all quantum interactions. Heavy particles can contribute as virtual particles to quantum loop corrections. As New Physics models contain very massive loop-contributing particles, these processes are probed by LHCb. The most promising decay to exploit New Physics is the $B_s^0 \rightarrow \mu\mu$ decay, in which the Z Boson decays into two muons (fig. 2.11b).

For more information on the LHCb physics program, see [19].

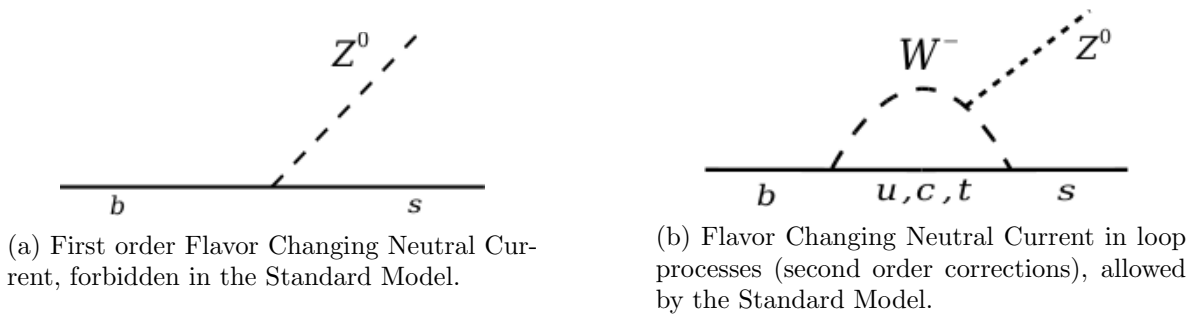


Figure 2.11: Flavor Changing Neutral Currents [1].

Chapter 3

Track Reconstruction at LHCb

Particles move through space along trajectories. Where charged particles interact with sensitive detector material, they leave *hits*. The hits are combined by software algorithms to form *tracks*. Tracks are straight or curved lines through the set of all recorded interaction points of a particle with the detector. The process of finding the track of a charged particle is called track reconstruction.

A track provides information about the position and the momentum of a charged particle. Combined with information on the particle type provided by the particle identification system, such a particle in the detector is fully described.

To define a track at a certain z -position, the following parameters are used:

- spatial coordinates in x and y direction,
- slope parameters $t_x = \frac{dx}{dz}$ and $t_y = \frac{dy}{dz}$,
- charge q and momentum p .

Using these quantities, a track is described by the state vectors $\vec{s}_i = (x, y, t_x, t_y, q/p)$ at several z -positions along the track (fig. 3.1). As only singly charged particles are regarded, the charge q is equal to ± 1 . The momentum is derived from the track curvature.

As described in section 2.2, before an event gets recorded, it has to pass the trigger requirements. One of the challenges of track reconstruction is the following: a proton-proton collision which generates a b hadron has about 50 other decay products, of which the trigger

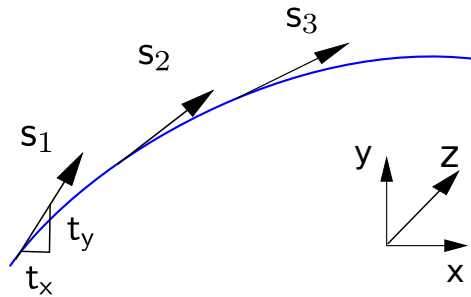


Figure 3.1: Sketch of a track with state vectors. The blue curved line represents a track in space; the s_i correspond to different points along the z -axis.

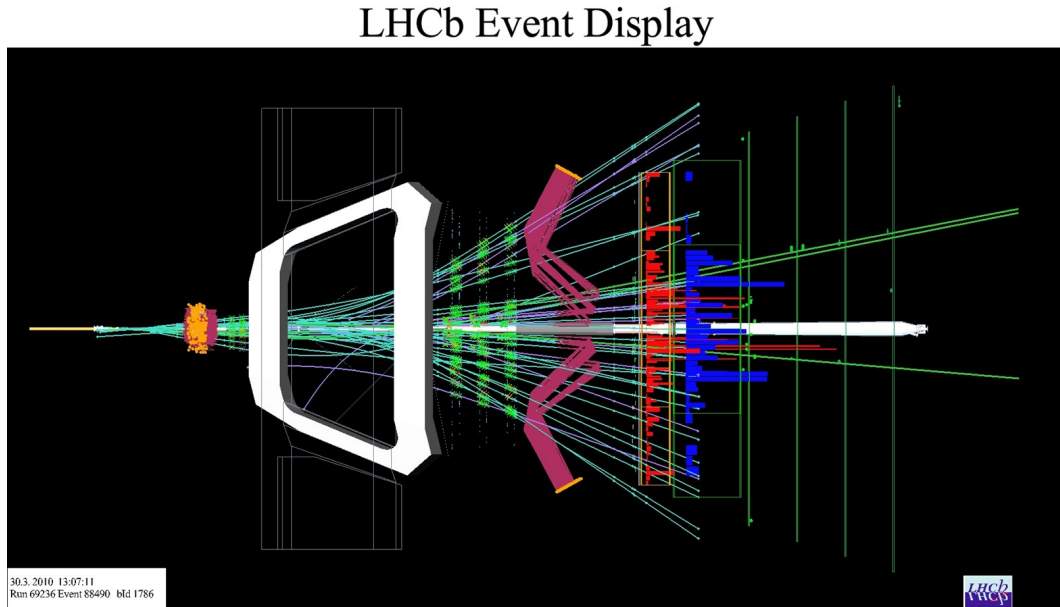


Figure 3.2: LHCb event display, view from above. The bent lines are particle tracks. The white horizontal line in the middle is the beam pipe, the white trapezoid illustrates the coil of the magnet. The Vertex Locator is situated at the far left-hand side. The displayed energies in the calorimeters are indicated by histograms. At right-hand side, three muons left signals in the muon stations [7].

has to extract the interesting b hadron. The trigger decision has to be taken as fast as possible. For this purpose, only particles with high transverse momentum and high transverse energy are reconstructed.

For physics analyses, entirely reconstructed decays are needed. The full reconstruction of a track is performed in three stages [18]:

- Pattern recognition: combining hits in one or more detectors to form a single track.
- Track fit: estimating track parameters which build the state vectors and calculating the associated errors.
- Removing fit failures and duplicate tracks. The latter are due to shorter versions of a longer track or to the same track being found twice by different algorithms.

Once this is done the full information of the event is accessible. The tracks are then visualized in the event display (fig. 3.2). They are represented by curved lines and their hits in the tracking station by points.

3.1 Track Types

Depending on the parts of the detector a particle traverses, the tracks are divided into the following types (fig. 3.3):

- *VELO tracks*: Tracks with hits in the Vertex Locator only. They usually have a large angle with respect to the beampipe. The particles causing such tracks left the angular

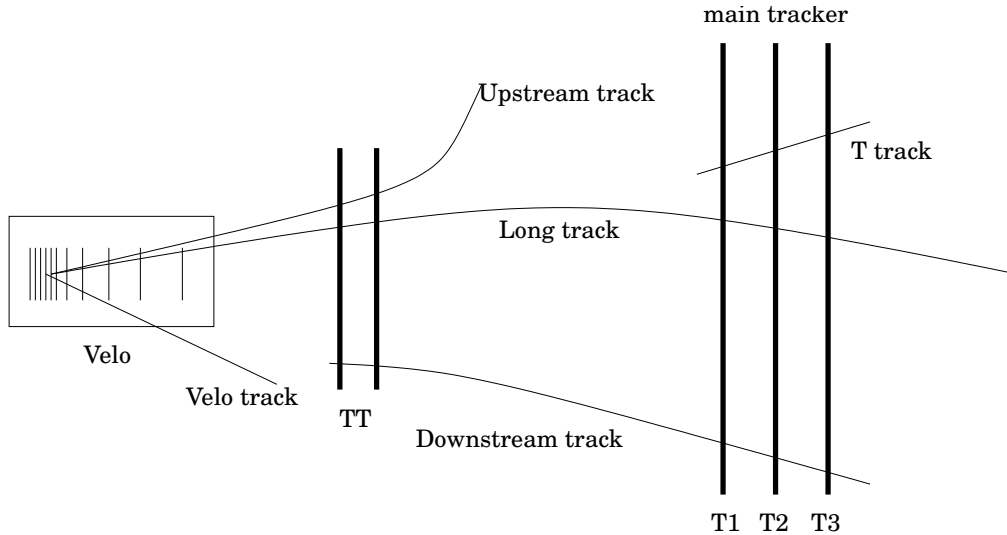


Figure 3.3: Illustration of the different track types in LHCb [7].

detector acceptance before reaching other detector parts. Also particles flying in the backward direction only leave VELO tracks.

- *Upstream tracks*: Hits are only produced in the Vertex Locator and the Trigger Tracker. Usually, upstream tracks are due to low momentum particles, which are bent out of the detector acceptance by the magnetic field after the Trigger Tracker.
- *Downstream tracks*: Tracks which have hits only in the Trigger Tracker and the tracking stations after the magnet. They often arise from charged decay products of long-lived resonances like the K_S^0 which decay outside of the Vertex Locator.
- *T tracks*: Tracks which can only be measured in the tracking stations after the magnet. Typically they originate from secondary interactions.
- *Long tracks*: The particle traverses the whole tracking system, leaving signals in both the Vertex Locator and all the Tracking stations. From these tracks, the most accurate information about the particle momentum can be extracted, because the particle passes through the whole magnetic field, leaving a track with a curvature that can be well measured.

3.2 Reconstruction Algorithms

Vertex Locator tracks and long tracks are the most important ones for the work of this thesis, therefore the reconstruction of these tracks is described in more detail in the following paragraphs.

3.2.1 Reconstruction of Vertex Locator Tracks

The magnetic field in the Vertex Locator is negligible. Hence, tracks in the Vertex Locator are considered as straight lines.

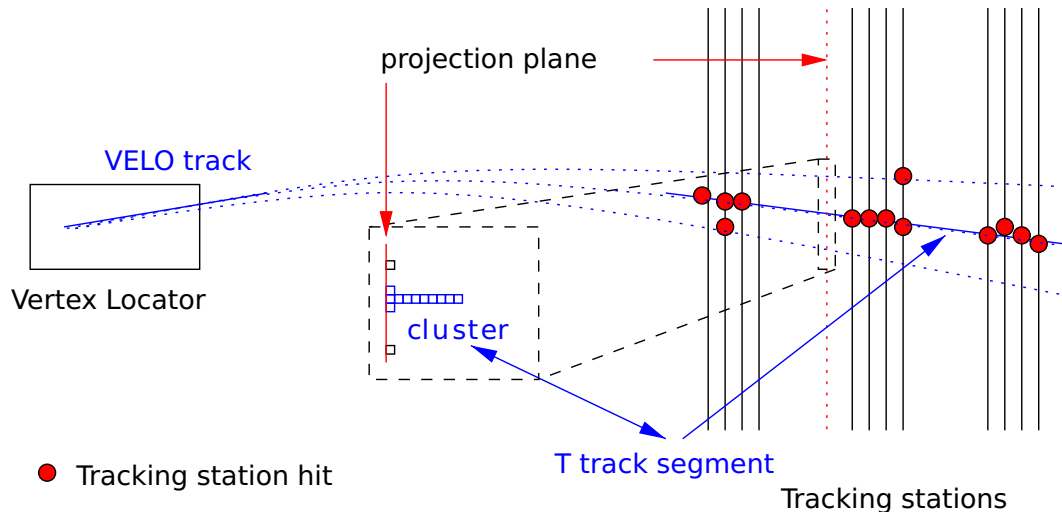


Figure 3.4: Sketch illustrating forward tracking using a Hough transform method. In the projection plane hits from the same VELO track form clusters [18].

There are two different approaches to find these tracks. The first one combines hits in the consecutive r - and Φ -sensor discs of the Vertex Locator before forming 3D tracks. The drawback of this method is that it is slow.

The second approach is split into two steps: first, only information of the r sensors is taken to form 2D tracks in an rz -projection. These 2D tracks are constrained to originate from the primary interaction region. They are then combined with the hits in the Φ sensors to get the 3D tracks [20].

3.2.2 Reconstruction of Long Tracks

In LHCb two different tracking algorithms are used for long track reconstruction.

One of the algorithms is called *forward tracking*. First a VELO track is combined with all hits in the tracking stations using a Hough transform method. The hits in the tracking station are projected onto a plane such that hits from the same VELO track form clusters.

The other algorithm is called *track matching*. This algorithm matches a VELO track and an already reconstructed T track. To determine, whether a T track is a good match to a VELO track, a χ^2 test is performed.

3.3 Reconstruction Software

To understand the differences between an analysis performed with Monte Carlo simulated data and an analysis performed with data taken in the LHCb experiment, it is important to have an idea of the workflow of the LHCb reconstruction software. Figure 3.5 summarizes the steps of event reconstruction.

Using LHCb data, the reconstruction procedure is straight forward: A collision takes place in the detector, leaving hits in the tracking detectors. From those, tracks are reconstructed and assigned to a particle type, called *reconstructed particles*.

Within a Monte Carlo simulation there are several steps needed. At first, a simulation of the physical properties are simulated, generating events and B decays. This process is called event generation. The simulated particles are called *Monte Carlo particles*. Then the

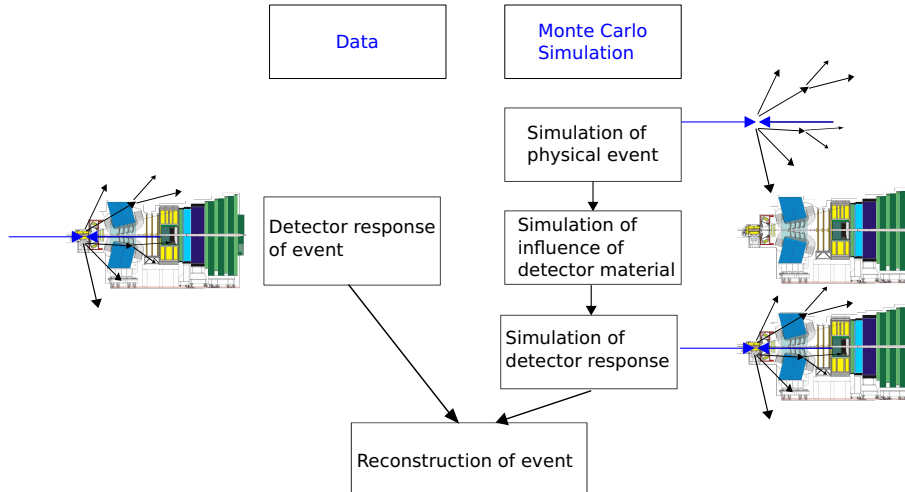


Figure 3.5: Workflow of the reconstruction software.

influence of the detector on this decay is evaluated. Interactions with detector material and the impact of the magnetic field are taken into account. The final step is to simulate the propagation of the particles through the detector and how the detector would respond to this event. The output of a simulated event has the exact same structure as the output of an event in the detector. Therefore, the particles can be reconstructed using the same software producing the same type of *reconstructed particles* as the reconstruction with data taken by LHCb.

Information about the decays of interest is collected and put together into files by a software framework called *DaVinci*.

3.4 Track Reconstruction Efficiency

As the track reconstruction efficiency is currently the largest systematic error on many measurements, there have been several studies estimating it [2]. These investigations address the problem of why some particles, which are *reconstructible*, are not *reconstructed*. It is important to emphasize the difference between reconstructible and reconstructed. A particle is considered as reconstructible, if certain requirements are met. The usual definition of reconstructible is:

- reconstructible in the Vertex Locator: the particle produced at least three hits in the r discs and three hits in the ϕ discs.
- reconstructible in the tracking stations: the particle produced at least one hit in a vertically arranged layer and one hit in a tilted layer within each station.
- reconstructible as long track: the particle is reconstructible in the Vertex Locator and in the tracking stations.

Using simulated data, it can be checked if these requirements are met by a certain Monte Carlo particle. Only if a particle is reconstructible, it can in fact be reconstructed by the

tracking algorithms. The fact that not every particle which is reconstructible really is reconstructed by the tracking algorithms leads to the definition of tracking efficiency of a simulation ϵ_{MC} as:

$$\epsilon_{MC} = \frac{\# \text{ of reconstructible tracks which are reconstructed}}{\# \text{ of all reconstructible tracks}} \quad (3.1)$$

This number gives the probability of reconstructing a charged particle which is reconstructible in the detector. It therefore describes how well the tracking algorithm works. However, the number of reconstructible particles cannot only be accessed in analyses using data taken by LHCb. In chapter 4 a data driven method will be introduced.

Chapter 4

Measurement of the Tracking Efficiency on Data Using the Decay Channel $B^+ \rightarrow J/\Psi K^+$

4.1 Introduction

The aim of LHCb is to measure asymmetries at the per mill level, therefore a precise knowledge of reconstruction efficiencies is of utmost importance. Not every particle traversing the detector is reconstructed. Reasons for particles not being reconstructed include the following:

- Hadronic interactions with the detector material (concerns only kaons, pions, protons): contribution of $\sim 15\%$ to the inefficiency [2].
- Inefficiencies of the tracking algorithms: contribute $\sim 5\%$.
- Large-angle scatterings: $\sim 1\%$ (for electrons much higher): particles scatter off material in a large angle and therefore fly out of the search window of tracking algorithms.

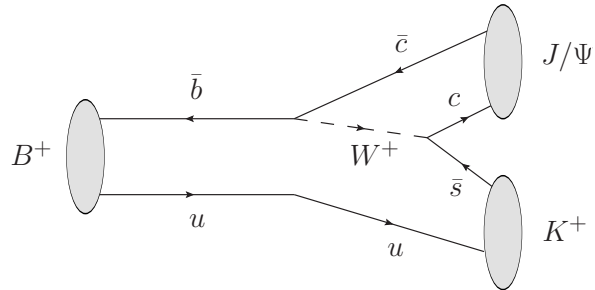
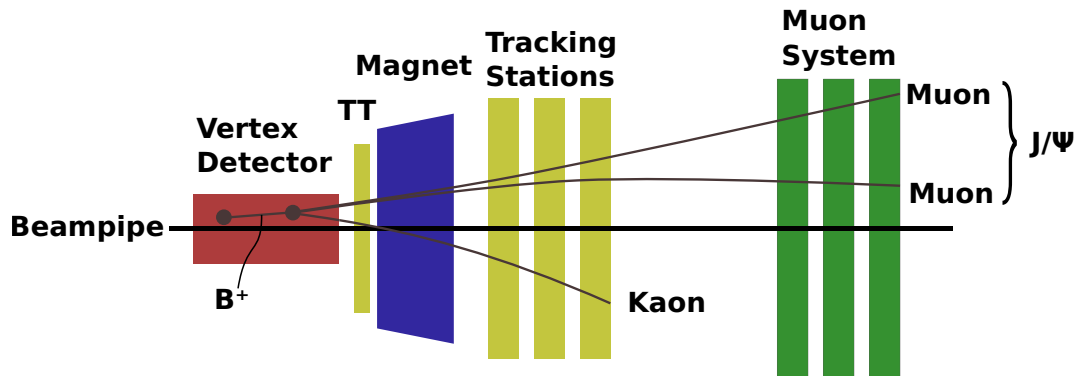
So far, the track reconstruction efficiency of LHCb has been determined taking only particles into account which traversed the whole detector. However, this approach does not account for inefficiencies due to interactions with detector material and decays in flight. The position and the amount of detector material is not known in all detail and therefore not entirely described by the simulation. Therefore the track reconstruction efficiency determined using simulation is different from data. Hence, a data driven analysis is required. In the following a data driven method calculating the reconstruction efficiency is presented.

The analysis was developed using $B^+ \rightarrow J/\Psi (\mu\mu) K^+$ decays (figs. 4.1 and 4.2): The B^+ decays into a kaon and a J/Ψ which again decays into two muons. ¹

The developed procedure is tested on simulation data. The advantage of simulated data is, that more information about the decay is accessible, which provides the opportunity of cross-checking the outcome of the analysis. Once the validity of the method is thereby established, the exact same algorithms are be applied to data taken by LHCb. The used data sample consisted of an integrated luminosity of 1 fb^{-1} of 2011 data².

¹Throughout this text $B^+ \rightarrow J/\Psi K^+$ also refers to its charge conjugate $B^- \rightarrow J/\Psi K^-$.

² $1 \text{ b}^{-1} = 10^{24} \text{ cm}^{-2}$

Figure 4.1: Feynman graph of a $B^+ \rightarrow J/\Psi K^+$ decay.Figure 4.2: Sketch of a $B^+ \rightarrow J/\Psi(\mu\mu)K^+$ decay in the LHCb detector (not to scale). Only the components of the detector which are relevant to track reconstruction of this decay are shown. The first and the second spots in the Vertex Locator mark the primary and the secondary vertex, respectively.

4.2 Track Reconstruction Efficiency Using Tag-And-Probe Methods

To obtain the track reconstruction efficiency using data taken in the LHCb, it is defined as:

$$\epsilon_{data} = \frac{\# \text{ of reconstructed tracks}}{\# \text{ of reconstructed tracks} + \# \text{ of not reconstructed tracks}} \quad (4.1)$$

This definition does not need the information about whether a particle is reconstructible as does eq. (3.1), thus the calculation can be applied both using simulations and data. However, it is not possible to know the number of tracks which did not get reconstructed at all. A first approach towards finding the reconstruction efficiency of the whole system is to restrict the problem to finding the reconstruction efficiency of a part of the system. In the here described analysis, this part is the Vertex Locator.

In the Vertex Locator there are also tracks are recorded which are not produced by a particle, but which are artifacts from reconstruction algorithms. These are called ghost tracks and make up about 12% of the tracks recorded by the Vertex Locator. Due to them, it is not possible to evaluate the track reconstruction efficiency by just looking for a matching long track for every VELO stub. The calculated invariant mass of the B^+ particle of a partially reconstructed $B^+ \rightarrow J/\Psi(\mu\mu)K^+$ is exploited to statistically separate true $B^+ \rightarrow J/\Psi K^+$ candidates from background and thereby exclude the Vertex Locator ghost tracks (sections 4.5 and 4.6).

For the efficiency calculation of partially reconstructed decays a tag-and-probe method is used. It does not rely on Monte Carlo information. The tracks used by the tag-and-probe method are referred to as legs. The tag leg is a fully reconstructed daughter particle of a decay, the probe leg is an only partially reconstructed daughter particle.

In this analysis the tag leg is provided by a J/Ψ particle. The J/Ψ particle of the $B^+ \rightarrow J/\Psi(\mu\mu)K^+$ decay instantly decays into two muons. Muons can penetrate a great amount of material, because they are unlikely to interact with matter. Due to their high mass (106 MeV) they travel a long distance before they are stopped by Bremsstrahlung. Additionally, they have a long lifetime of 2.2 μ s. For these reasons they are regarded as stable within the detector. Together with the fact that they are the only particles which are detected in the muon chambers, their reconstruction is straight forward. By combining them, the J/Ψ particle is found.

The kaon is more likely to interact with matter, thus the probability for it not to being reconstructed is higher. Therefore it provides the probe leg. In this analysis, the probe leg is the Vertex Locator part of a longer track. The short part in the VELO of a longer track is called *VELO stub*.

The whole decay is reconstructed by combining the probe leg and the tag leg. It is needed to find the VELO stubs which are most probably belonging to a kaon. How this is done will be described in detail in section 4.3.

The track reconstruction efficiency can be calculated by searching for reconstructed long track corresponding to the probe leg. If a corresponding long track is found the probe leg is defined as reconstructed, VELO stubs without a corresponding long track are not reconstructed as a long track. The reconstruction efficiency in the tracking stations can be defined as:

$$\epsilon_{data} = \frac{\# \text{ of reconstructed probe legs}}{\# \text{ of reco. probe legs} + \# \text{ of not reco. probe legs}} \quad (4.2)$$

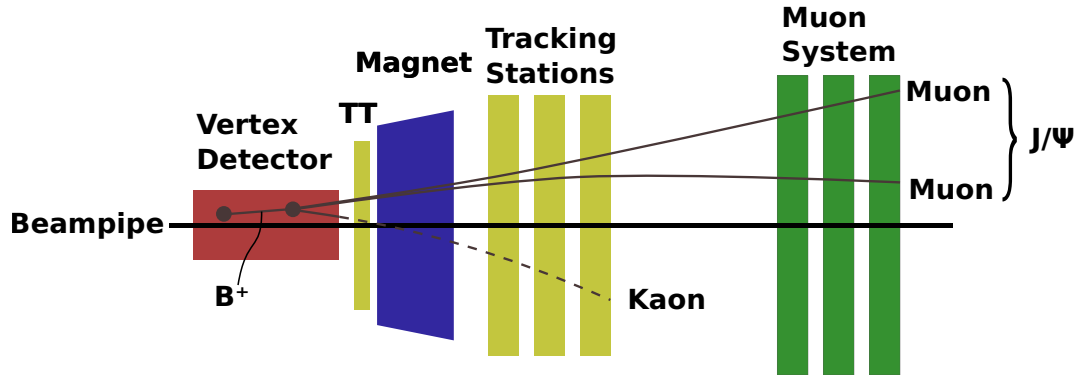


Figure 4.3: Compared to fig. 4.2, here the dashed kaon line represents the detector information suppressed if only the VELO stub of the kaon is taken into account.

4.3 Reconstruction of $B^+ \rightarrow J/\Psi K^+$ with Partially Reconstructed Kaons

In section 4.2, it is explained in order to evaluate the track reconstruction efficiency in the presented analysis, it is necessary to combine VELO stubs and J/Ψ long tracks. The developed method to reconstruct the $B^+ \rightarrow J/\Psi K^+$ decay using partially reconstructed kaons is described in the following.

The primary vertex, which is the B^+ production vertex is formed by tracks reconstructed in the Vertex Locator. The other tracks contributing to the investigated $B^+ \rightarrow J/\Psi K^+$ decay are detected as two long tracks left by the two daughter muons of the J/Ψ particle, and a VELO stub of the kaon (fig. 4.3).

For a full reconstruction of a decay, the momenta of the particles have to be known. As described in section 2.1, the particles traverse a magnetic field. Composing the slope of the track in the Vertex Locator before the magnet and the slope in the tracking stations after the magnet allows to determine the momenta. Hence, as only the part of the track in the Vertex Locator is used for the probe leg, no momentum information about the particle is available. The only information which can be derived using only the Vertex Locator is the probe particle's flight direction. In this analysis it is denoted \vec{e}_K , as the VELO stub belonging to a kaon is searched.

The mean lifetime of the B^+ particle is 1.6×10^{-12} s, which leads to a decay length of about 1 cm in the LHCb detector. This distance is too short for the particle to leave the Vertex Locator, therefore also for the B^+ particle no momentum information is accessible. The flight direction of the B^+ particle, \vec{e}_{B^+} is determined by subtracting the spatial coordinates of the B^+ production vertex (primary vertex) from the B^+ decay vertex (secondary vertex). Since the mean lifetime of the J/Ψ is negligible, its only vertex is the B^+ decay vertex.

Of the J/Ψ particle, the whole momentum information $p_{J/\Psi} \vec{e}_{J/\Psi}$ is available, where $p_{J/\Psi}$ denotes the magnitude of the momentum and $\vec{e}_{J/\Psi}$ denotes the flight direction.

The decay is only fully described if the momenta of *all* particles in the decay are known. If the momenta are put into the law of momentum conservation, an equation with two unknown variables, p_{B^+} and p_K resides:

$$p_{B^+} \vec{e}_{B^+} = p_{J/\Psi} \vec{e}_{J/\Psi} + p_K \vec{e}_K \quad (4.3)$$

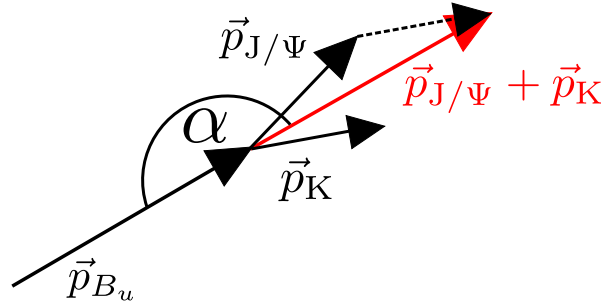


Figure 4.4: Visualization of the momentum vectors of a $B^+ \rightarrow J/\Psi K^+$ decay, and the angle used in eq. (4.6). To keep the sketch simple, $p\vec{e}$ is rewritten as \vec{p} . The dashed vector represents the kaon momentum vector shifted in parallel.

The additional information needed to evaluate all variables is obtained with the scalar product:

$$\vec{a} \cdot \vec{b} = |\vec{a}||\vec{b}| \cos(\alpha) \quad (4.4)$$

The B^+ direction vector and the vector resulting from adding the J/Ψ momentum and the kaon momentum (fig. 4.4) are plugged into eq. (4.4):

$$\vec{e}_{B^+} \cdot (p_{J/\Psi} \vec{e}_{J/\Psi} + p_K \vec{e}_K) = |\vec{e}_{B^+}| \cdot |p_{J/\Psi} \vec{e}_{J/\Psi} + p_K \vec{e}_K| \cos(\alpha) \quad (4.5)$$

Rewriting it leads to:

$$\cos \alpha = \frac{\vec{e}_{B^+} \cdot (p_{J/\Psi} \vec{e}_{J/\Psi} + p_K \vec{e}_K)}{|\vec{e}_{B^+}| \cdot |p_{J/\Psi} \vec{e}_{J/\Psi} + p_K \vec{e}_K|} \quad (4.6)$$

If the cosine equals 1, both the B^+ vector and the combined vector point to the same direction, which is a necessary condition for momentum conservation.

Equation (4.6) only relies on p_K as unknown variable. By extreme value calculation maximizing $\cos(\alpha)$ the solutions for p_K are found (appendix B).

4.4 Event Selection

There are several sources of background in the reconstruction of $B^+ \rightarrow J/\Psi K^+$ decays using partially reconstructed kaons.

- Combinatorial background: before particle identification, tracks are combined to form decays, however sometimes tracks are combined which do in fact not belong to the same decay.
- Partially reconstructed multiple branching decays: only a part of a decay with several decay products is reconstructed
- Physical background: tracks are identified with the wrong particle leading to the reconstruction of a decay which is different from the one it actually is.
- VELO stubs not belonging to a kaon: As mentioned, the presented analysis the $B^+ \rightarrow J/\Psi K^+$ decay is reconstructed using of a J/Ψ long track and a VELO stub. However, there are numerous VELO stubs in an event belonging to other particles than kaons.

To reduce background several selection cuts are applied. These are divided into pre-selection cuts and final cuts. The aim of the pre-selection cuts is to apply loose cuts which reduce statistics while keeping the candidates of interest. The final cuts are tighter to further improve the signal-to-background ratio.

The evaluation of the best value of the cuts is performed with a Monte Carlo sample. The used Monte Carlo sample is a J/Ψ inclusive sample, which consists of particles that decay into a J/Ψ particle plus one or several other particles. The conventions used in this chapter are that in order to be considered as a signal candidate, the candidate has to be a *Monte Carlo truth matched* $B^+ \rightarrow J/\Psi K^+$ decay. This means, to all given reconstructed particles in the decay and to the reconstructed VELO stub there exists an associated Monte Carlo simulated particle. The condition for a Monte Carlo particle regarded in this selection to be associated to a reconstructed particle is that they have 70 % of the hits in common.

The cuts are iteratively varied, after each step checking how many signal and how many background events are left. At the best signal-to-background ratio, the value for the cut is fixed. Table 4.1 at the end of this chapter summarizes the applied cuts.

In the following, the used selection cuts are described. Due to performing the analysis with VELO stubs it is not sufficient to apply only the in particle physics well-established cuts. At first, custom-made cut quantities will be explained detail. Afterwards, some in particle physics well-established cuts are briefly described.

4.4.1 Custom-Made Cuts

Track-Vertex-Distance

If a VELO stub is produced by the kaon from the $B^+ \rightarrow J/\Psi K^+$, it originates from the J/Ψ vertex. Taking this fact as an approach to find the correct VELO stubs, a cut is applied to the distance between the J/Ψ vertex and the VELO stub.

The track-vertex-distance cut is the most efficient cut. On a test sample of 1.47 million $B^+ \rightarrow J/\Psi K^+$ candidates and with a value of 0.6 mm for the cut the total number of candidates is reduced by 71.0%, while leaving 99.5% of the signal events. Additionally, it can

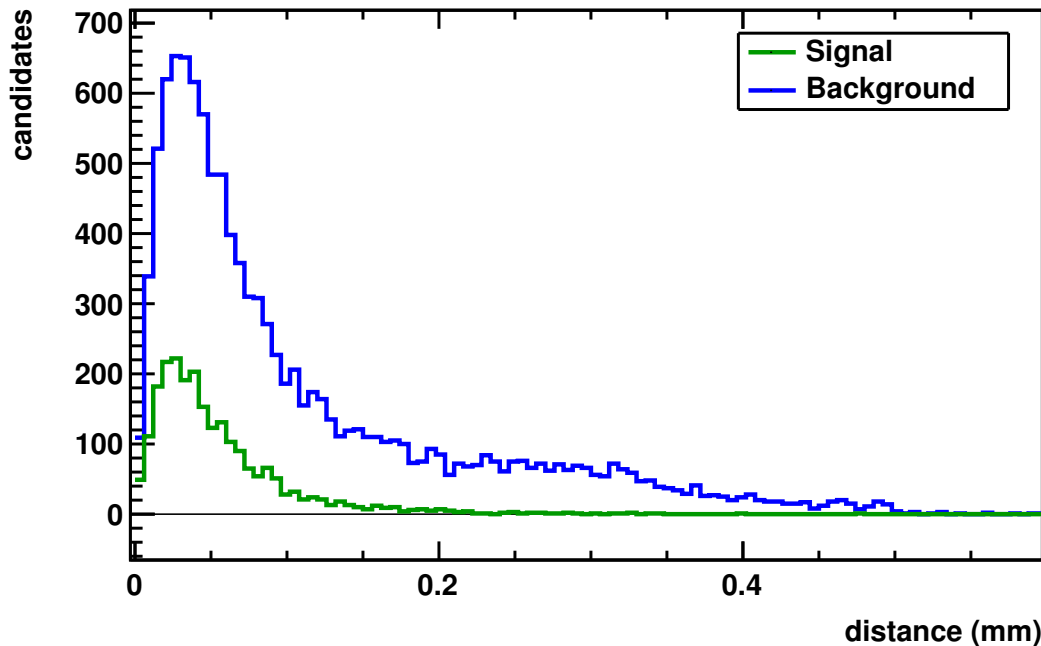


Figure 4.5: Histogram showing the distance between the J/Ψ vertex and the kaon VELO stub for Monte Carlo truth matched $B^+ \rightarrow J/\Psi K^+$ candidates (signal) and other candidates in the J/Ψ inclusive sample (background). All other cuts are applied. As the cut of 0.5 mm is applied before the analysis, no data exceeding this value can be shown in the plot.

be computed very fast. Due to the good performance of the cut at low computation time, it is put into the pre-selection, reducing the computation time of the analysis.

Figure 4.5 shows the track-vertex-distance for Monte Carlo truth matched $B^+ \rightarrow J/\Psi K^+$ candidates (signal) and other candidates in the J/Ψ inclusive sample (background). The plot was produced with all other cuts applied. From the low background distribution, it can be seen that some of the other cuts reduce background in the same regime. However, its application as a pre-selection cut is justified due to its fast computation time, as less data is left to be dealt with by the final cuts.

For the analysis, the VELO stub with the smallest track-vertex-distance is taken as candidate for the kaon.

Clone Cut

As there is no information available about the particle type a VELO stub belongs to, it is possible that the VELO stub assigned to a kaon by the analysis, in fact belongs to one of the muons of the J/Ψ particle. If one particle is reconstructed with two tracks, these are called clones. It is necessary to apply a cut rejecting clones. The chosen requirement for this cut is, that within a small opening angle around the kaon track, there is no other track. Otherwise the candidate is rejected.

As the clones represent the same particle, the angle between them is theoretically vanishing (fig. 4.6). An upper boundary of the angle of 0.001° is determined, where background is reduced and the signal events are hardly affected.

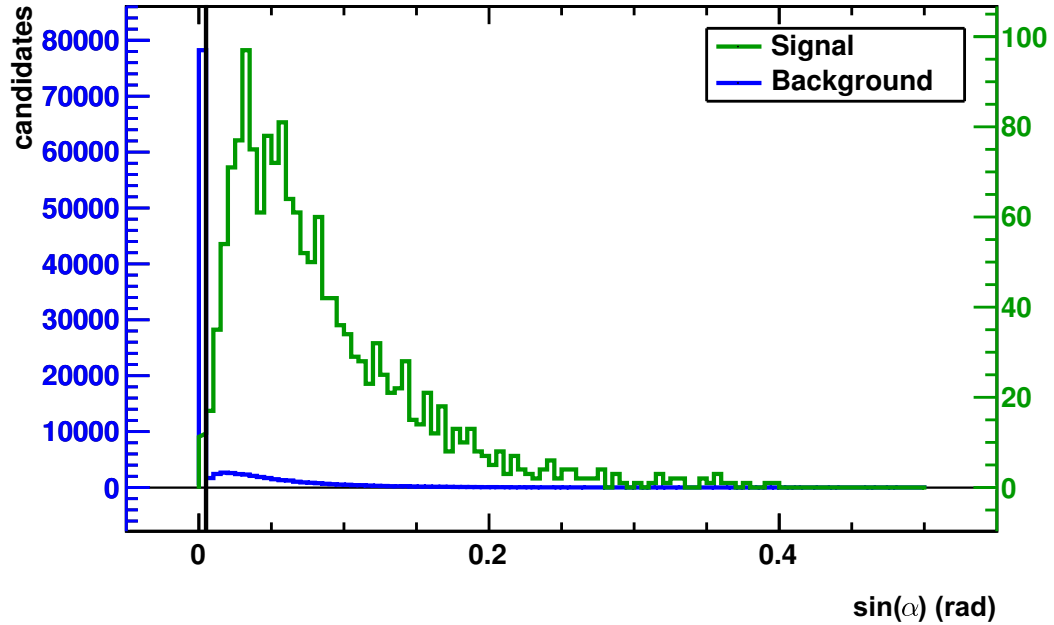


Figure 4.6: Histogram showing the sine between a VELO track and its closest neighbor for Monte Carlo truth matched $B^+ \rightarrow J/\Psi K^+$ events (signal) and all the other candidates of the J/Ψ inclusive sample (background). The high background peak at 0 results from clones. The value of the cut is 0.001. Left axis: scale for background, right axis: scale for signal. The vertical line represents the cut.

Track Isolation

A kaon of a $B^+ \rightarrow J/\Psi K^+$ event flies isolated from other particles. Hence to find the right VELO stub, only those are of interest, for which there are no other tracks in the close vicinity.

The VELO stub which is second closest to the J/Ψ vertex is searched. Only if its distance with respect to the J/Ψ vertex is bigger than the chosen cut value, the decay is kept (fig. 4.7). In fig. 4.8 the distance of the second closest track is shown for signal and background. This plot demonstrates that in background the second closest track is in closer vicinity of the J/Ψ vertex than for signal. In this plot, all other cuts are applied. However, the value for this cut is obtained without any other cuts applied. Background candidates which are expected to be filtered out by the isolation cut are already suppressed by other cuts. This circumstance was discovered after finishing the analysis. For future analyses a cut of about 0.1 mm is recommended.

The clone-cut and the isolation cuts are similar. However, the difference is that the clone-cut searches in the vicinity of a track for a second track, whereas the isolation cut investigates the vicinity of the J/Ψ vertex. Nevertheless, these two cuts are highly correlated. If a track is within the cut radius of the isolation cut and has a clone, the event is not only vetoed by the clone-cut, but also by the isolation cut, because the second closest track (the clone) is automatically within the cut radius.

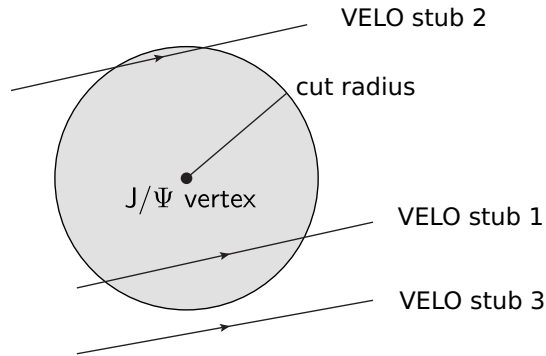


Figure 4.7: Sketch visualizing the isolation cut. Only if the distance between the second closest VELO stub and the J/Ψ vertex is bigger than the cut radius, the decay passes the requirements of the isolation cut. The decay belonging to this sketch would be vetoed, as the second closest VELO stub (number 2) is still within the cut radius.

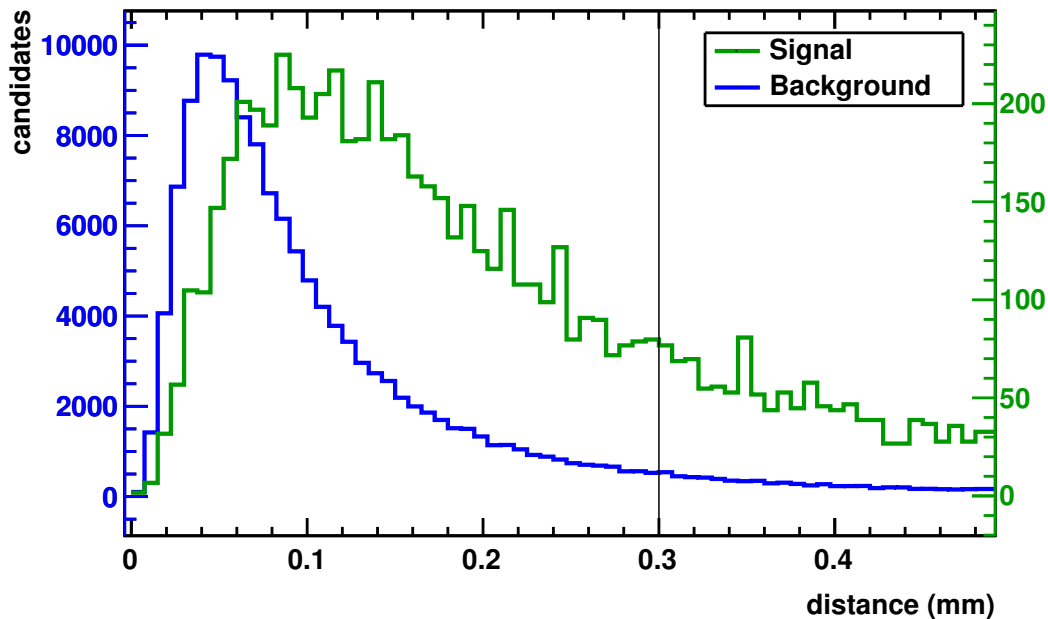


Figure 4.8: Histogram showing the distance of the second closest track for Monte Carlo truth matched $B^+ \rightarrow J/\Psi K^+$ candidates (signal) and other candidates in the J/Ψ inclusive sample (background). Left axis: scale for background, right axis: scale for signal. The vertical line indicates the cut. All other cuts are applied. Value used for cut is 0.3 mm.

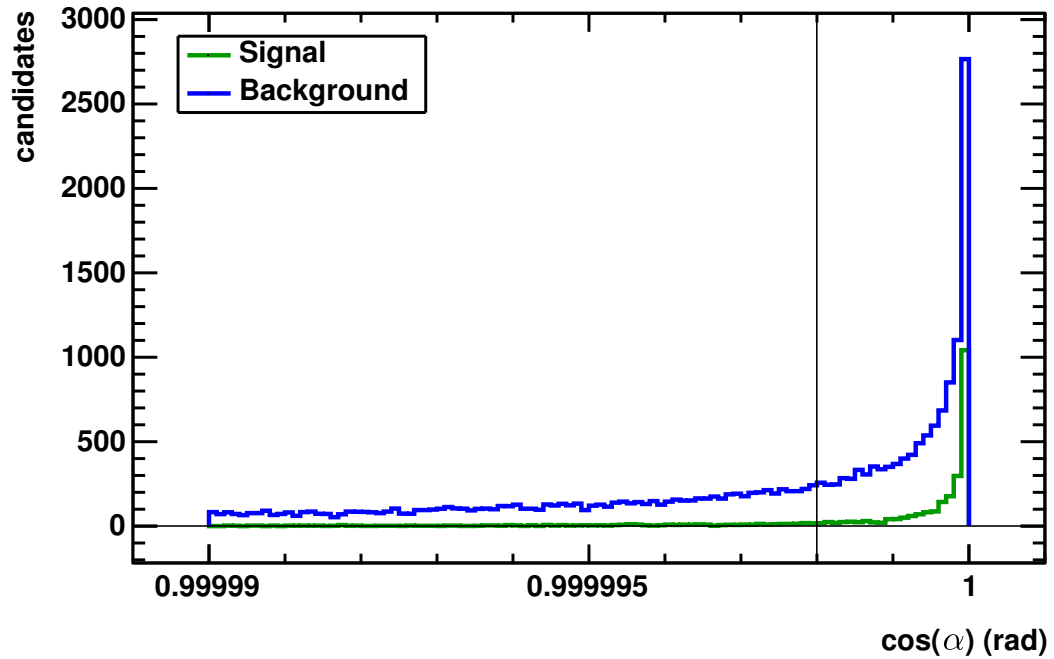


Figure 4.9: Cosine of the maximized angle showing Monte Carlo truth matched $B^+ \rightarrow J/\Psi K^+$ candidates (signal) and other candidates in the J/Ψ inclusive sample (background). The vertical line indicates the cut. All other cuts applied. Histogram generated after requiring that a maximal cosine exists. Value used for cut is 0.999998.

Cosine of Maximized Angle

With the method of calculating the B^+ mass with a kaon VELO stub, the angle between the B^+ momentum, and the combined momentum of the kaon and the J/Ψ is maximized (section 4.3). The cosine of the angle does not get set to 1 because due to inaccuracies obtaining an exact value of 1 is unlikely (fig. 4.9). To avoid keeping candidates with a cosine of the maximal angle completely different than 1, a cut on the angle has to be applied.

4.4.2 Standard Cuts

Vertex χ^2

The vertex χ^2 is an estimate of the validity of the decay vertex of a particle. It is defined as $\chi^2 = (D/\sigma_D)^2$, D denotes the distances of all the tracks of the daughter particles with respect to the decay vertex of the mother particle. The difference between the cut on the J/Ψ + VELO stub vertex χ^2 and the track-vertex-distance cut is, that calculating the χ^2 is very CPU-consuming.

Significance of the B^+ Flight Distance

The mean flight distance of a B^+ particle in the Vertex Locator is about 1 cm. Instead of the distance itself the significance of the distance is taken as value on which the cut is applied. The significance is the value divided by its error and therefore a measure of the reliability

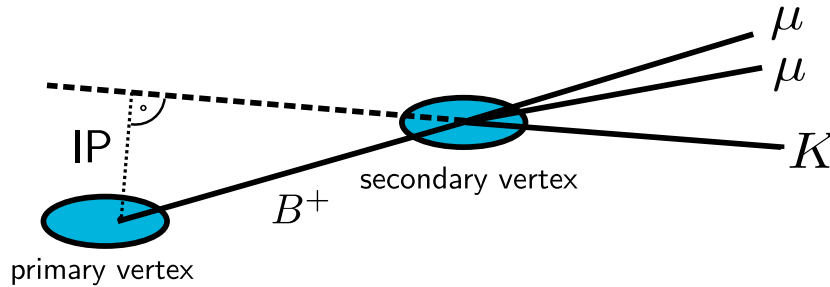


Figure 4.10: Sketch of the impact parameter (IP), which is represented by the dotted line. The dashed line is a backward extension of the kaon VELO stub. The smaller the impact parameter, the higher the possibility a particle stems from the primary vertex.

Cut	Value
Pre-Selection	
J/ Ψ mass	± 80 Mev
VELO stub: track-vertex-distance	< 0.5 mm
additionally on data	
J/ Ψ transverse momentum	> 500 Mev
J/ Ψ vertex χ^2	± 20 Mev
Final Selection	
sine clone angle	> 0.001 rad
track isolation	> 0.3 mm
cosine maximum angle	> 0.999998 rad
J/ Ψ + VELO stub vertex χ^2	< 0.2
B^+ flight distance significance	> 5
impact parameter kaon significance	> 3
VELO stub pseudorapidity	> 3.2

Table 4.1: Cuts applied to $B^+ \rightarrow J/\Psi K^+$ samples.

of this value. Cutting on the significance gives a better separation of signal and background than the absolute value.

Significance of the Impact Parameter of the VELO Stub

The impact parameter is defined as the perpendicular distance from a track to the primary vertex (fig. 4.10). A cut on the impact parameter separates particles produced at the primary vertex and particles produced at displaced vertices. The smaller the impact parameter the higher the possibility a particle stems from the primary vertex. A cut is applied to the significance of the impact parameter of the VELO stub.

VELO Stub Pseudorapidity

VELO stubs with a low pseudorapidity η and therefore large angle with respect to the beam pipe tend to leave the detector acceptance. Therefore the probability for them not being reconstructed as long tracks is high. The cut is applied to keep high-pseudorapidity candidates.

4.5 B^+ Mass Distribution

In section 4.3 it is explained how to obtain the whole momentum information of the partially reconstructed $B^+ \rightarrow J/\Psi K^+$ decay. Using the obtained momenta, it is possible to calculate the invariant mass of the B^+ particle. In the following, the resulting mass peaks are shown with the full selection applied (section 4.4). They are used to separate statistically signal and background events later in the analysis.

The method to find the track reconstruction efficiency is first performed with simulated data. The procedure with simulated data is divided into two consecutive steps. First the routine is applied to a sample only containing $B^+ \rightarrow J/\Psi K^+$ events for the purpose of developing the method without having to deal with background. Next the procedure is applied to a J/Ψ inclusive sample. In this sample a particle decays into a J/Ψ particle and one or several other particles. It provides a structure similar to data taken in the LHCb experiment, while still having access to Monte Carlo information. Therefore cross-checks are possible for verification of the analysis method. In the end, the method is applied to data taken by LHCb.

4.5.1 Monte Carlo $B^+ \rightarrow J/\Psi K^+$ Sample

At first, a Monte Carlo $B^+ \rightarrow J/\Psi K^+$ sample is taken, in which all VELO stubs in the decay are assigned to a kaon mass hypothesis by construction. The only background in this sample is combinatorial background.

In fig. 4.11, the B^+ invariant mass histogram obtained with the method using partially reconstructed decays is plotted without cuts applied. For fig. 4.12, all selection cuts are applied. Despite both signal and background candidates are reduced (to be seen when comparing the scale on the y-axis of fig. 4.12), the background candidates are reduced much more than the signal candidates. The hereby obtained signal peak is fitted with a combination of two Gaussian curves (double-Gaussian), the background with an exponential curve.

The signal peak is found at 5281.14 ± 0.29 MeV. Comparing it with the known value for the B^+ mass shows that the method using partially reconstructed decays is a valid procedure for the reconstruction of a $B^+ \rightarrow J/\Psi K^+$ decay.

4.5.2 Monte Carlo J/Ψ inclusive Sample

For Monte Carlo studies, a J/Ψ inclusive sample of about 830 000 events is used. As already mentioned, the mother particle of this decay channel decays into a J/Ψ particle plus one or several other particles. As only B decays have a displaced J/Ψ vertex and leave a clear signature, it is possible to take these displaced vertices as the only trigger condition. The J/Ψ inclusive background is twofold: Either a B^+ is found, but a wrong track is picked for the kaon. Or a decay with any any mother particle is taken. A Monte Carlo J/Ψ inclusive sample has a background similar to the one in data. Because of this behavior, it is taken as a first approach towards the analysis on data.

With all cuts of table 4.1 applied, fig. 4.13 is obtained. With Monte Carlo information, it is possible to extract the signal peak by Monte Carlo truth matching. Even though a signal peak is visible, the background is not just an exponential stemming from combinatorics. Investigating the background composition using Monte Carlo information reveals that the signal shape is due to decays which cannot be subtracted with cuts. The two dominant decays apart from the wanted $B^+ \rightarrow J/\Psi K^+$ decay are:

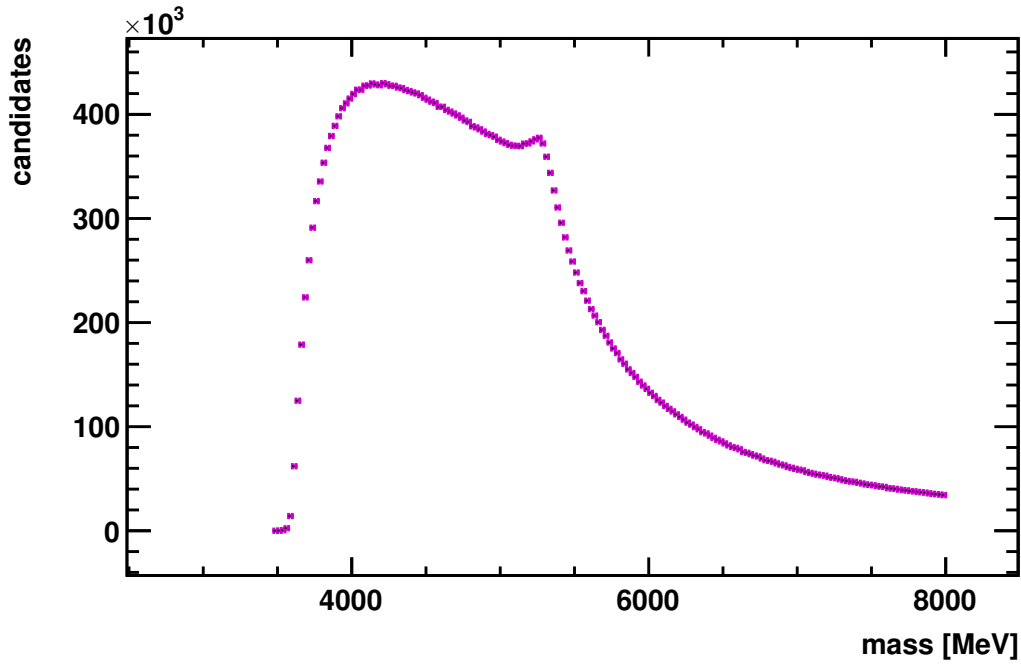


Figure 4.11: Histogram of the B^+ mass of partially reconstructed $B^+ \rightarrow J/\Psi K^+$ decays in a Monte Carlo simulated $B^+ \rightarrow J/\Psi K^+$ sample. Only pre-selection cuts are applied.

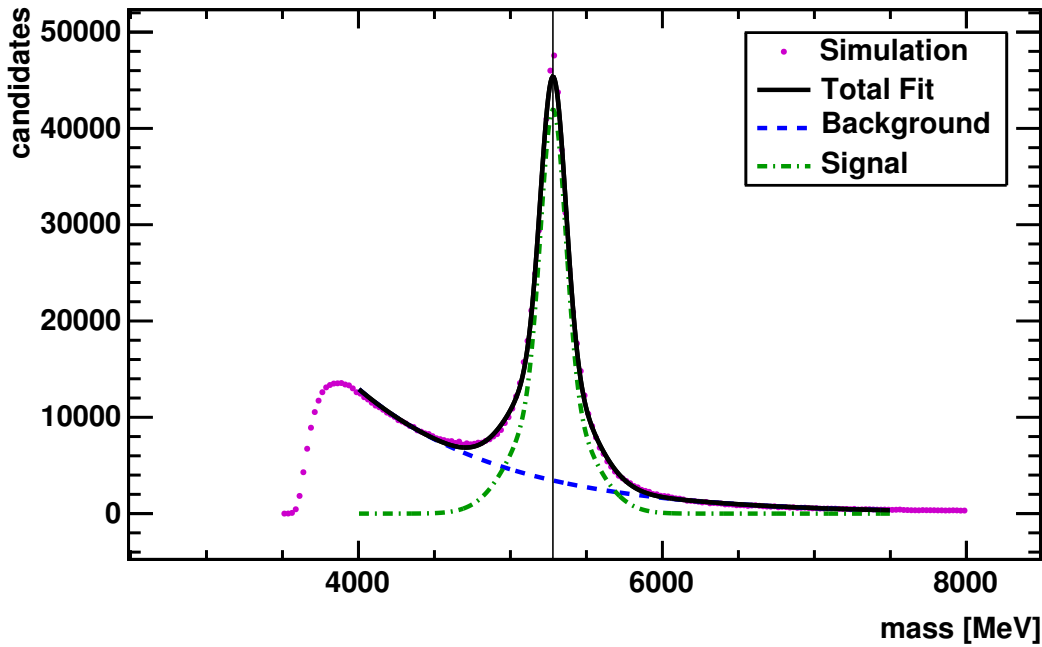


Figure 4.12: Same Monte Carlo simulated $B^+ \rightarrow J/\Psi K^+$ sample as in fig. 4.11, with final cuts applied. The position of the $B^+ \rightarrow J/\Psi K^+$ candidate signal peak is at 5281.14 MeV, with a root mean square of 0.29 MeV.

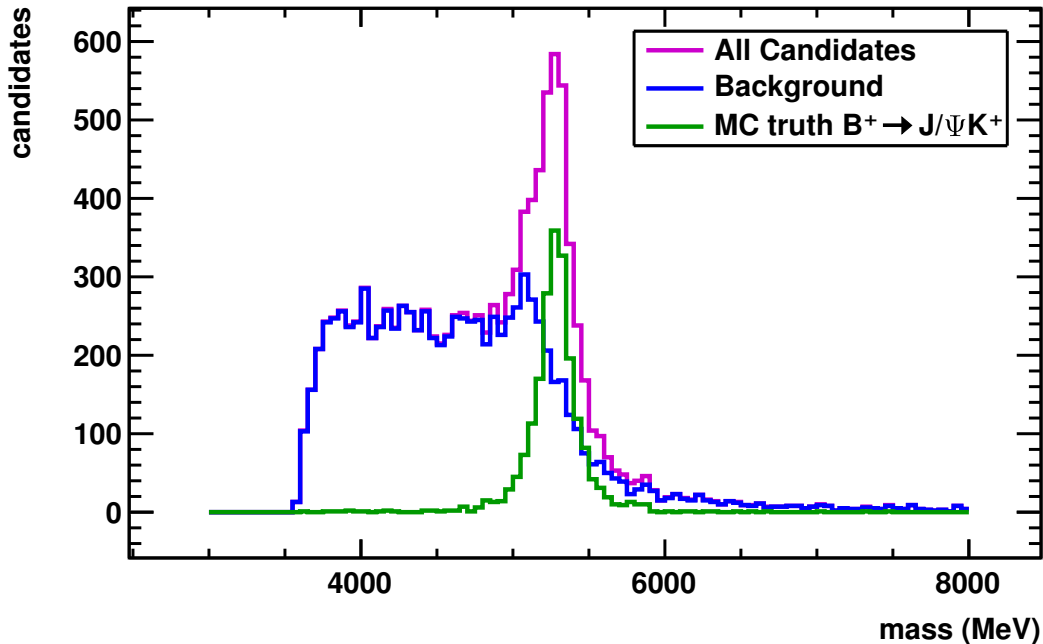


Figure 4.13: Histogram of the B^+ mass for partially reconstructed $B^+ \rightarrow J/\Psi K^+$ decays in a Monte Carlo J/Ψ inclusive sample, after final cuts. The signal peak contains only Monte Carlo truth matched $B^+ \rightarrow J/\Psi K^+$ candidates, the residing events are considered as background. The signal peak's mean lies at 5279 MeV, with a root mean square of about 220 MeV.

- $B^+ \rightarrow \Psi(2S) K^+$;
 $\Psi(2S)$ is an excited state of the J/Ψ particle and decays into a J/Ψ particle and a neutral particle.
- $B^+ \rightarrow J/\Psi K^{*+}(892)$;
 $K^{*+}(892)$ is an excited state of the kaon and decays into a K^+ and a π^0 .

The major problem arose from the background due to $B^+ \rightarrow J/\Psi K^{*+}$ decays. The calculated mass peak obtained with the K^{*+} decay is within the range of the signal peak obtained with the $B^+ \rightarrow J/\Psi K^+$ events (fig. 4.14). They can only be separated, if Monte Carlo truth information is accessible.

4.5.3 Data Sample

The used sample of data taken in the LHCb experiment contains about 195 000 events. The method to evaluate the B^+ mass used for the Monte Carlo J/Ψ inclusive sample is applied in the same way to data. As expected, the obtained mass distribution is similar to the results of the J/Ψ inclusive sample (fig. 4.15).

Using data, other methods than Monte Carlo truth matching have to be applied to distinguish between signal and background. A first approach is subtracting the mass histogram of background obtained using the J/Ψ inclusive analysis from the data distribution. However, as the distributions are not smooth, fluctuations of the number of candidates per bin in the histograms did not cancel each other out, leading to a resulting histogram with even higher fluctuations.

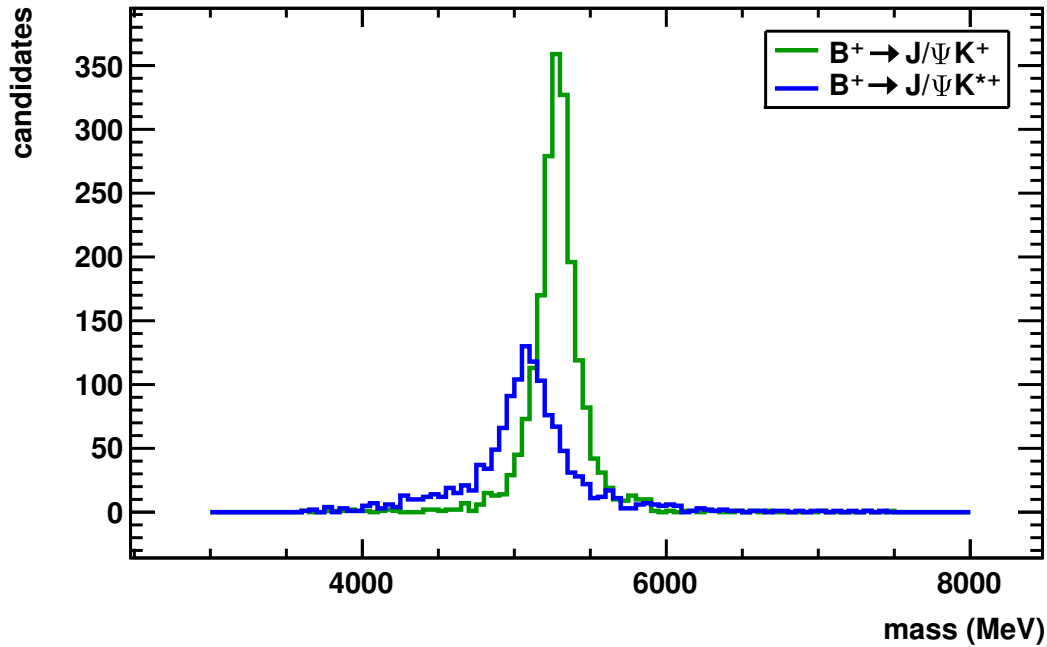


Figure 4.14: Detailed view of the data shown in fig. 4.13. The $B^+ \rightarrow J/\Psi K^+$ peak is the same as in fig. 4.13, the $B^+ \rightarrow J/\Psi K^{*+}$ peak is extracted from the background distribution in fig. 4.13. The mean value of the $B^+ \rightarrow J/\Psi K^{*+}$ peak is 5079 MeV, with a width of about 410 MeV.

It turned out that a better procedure is to first fit the B^+ mass distribution of the J/Ψ inclusive sample and take the fit function of the background as input to fit the histogram of data. Some of the fitting parameters are used in the efficiency calculation, therefore the procedure is discussed in more detail in the next section.

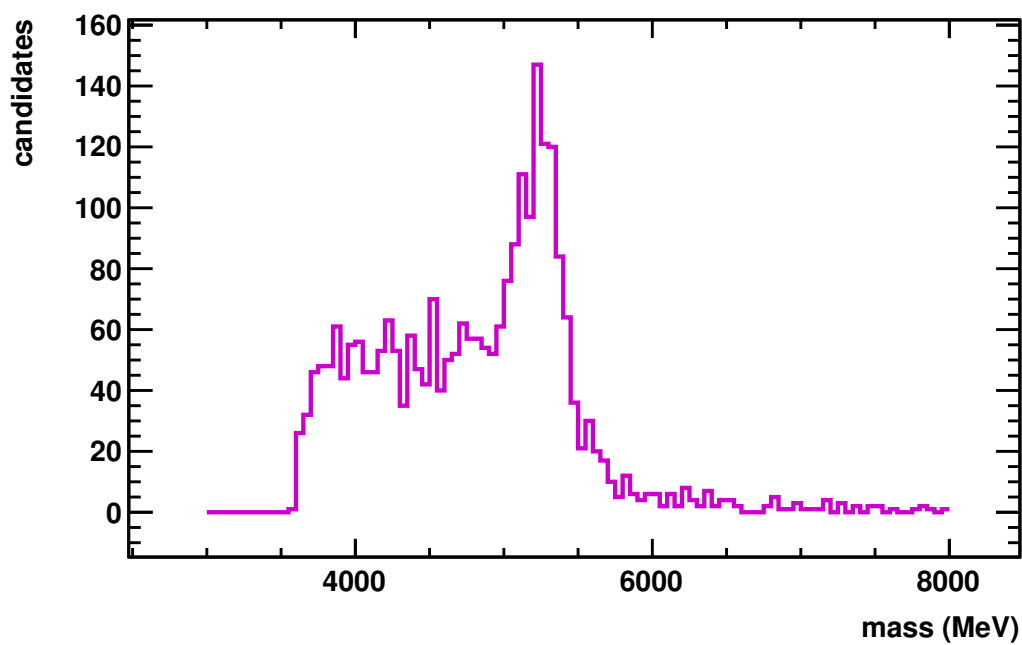


Figure 4.15: B^+ mass distribution using partially reconstructed $B^+ \rightarrow J/\Psi K^+$ decays on data, after final cuts.

4.6 Efficiency Calculation

Once a histogram with clear B^+ mass peak is obtained, the track reconstruction efficiency can be calculated. However, to get the appropriate input, some computations are necessary as described in the following paragraphs.

4.6.1 Long Track Matching

In the here described analysis, VELO stubs which are not reconstructed as a long track are defined as *not reconstructed* particles. On the other hand, particles which have a long track matching the VELO stub are *reconstructed*.

The starting point is the assumption that every kaon is detected in the Vertex Locator, but it is not initially known, if they are also reconstructed as a long track. To match the VELO stubs with their according long tracks, the cosine between a VELO stub and all available long tracks are calculated. If it is bigger than 0.99999 and therefore the angle close to 0, the long track is considered to be the match for the VELO track.

4.6.2 Signal - Background Separation

Additionally to searching long tracks matching the VELO stubs, it is important to statistically separate the B^+ mass distribution into true $B^+ \rightarrow J/\Psi K^+$ decays (signal) and background due to misidentified decays, combinatorics and clones of the kaon VELO stub. The statistical methods have to be applied which are described in the following.

Fitting The B^+ Mass Distribution

At first, the background had to be fitted. Using data taken in the LHCb experiment there is no direct way of separating signal from background, because no information on the particle identity of the VELO stub is available. A way of distinction is by the shape of the B^+ mass distribution. In general, an exponential decay is identified with combinatoric background, so if the whole mass distribution is an exponential curve with a peak on top, the identification of signal and background is straight forward: The part of the fit which represents the peak is identified with signal candidates and the exponential curve with background.

The background shape of the $B^+ \rightarrow J/\Psi K^+$ decay is not exponential, even after applying all possible cuts to reduce background (section 4.5). This indicates the presence of physical background.

The fitting of signal and background is divided into two steps: At first, a Monte Carlo sample is used. Hence the information about the particle type of each track is accessible via Monte Carlo truth information. Signal could be distinguished from background by looking for Monte Carlo truth matched $B^+ \rightarrow J/\Psi K^+$ decays. All the other events are plotted collectively as a background histogram and a fit is searched which best describes its shape. The adjustment used for fitting is the χ^2 method implemented in *ROOT*. The best fit turned out to be an exponential and two Gaussian curves. The fit range is chosen such that boundary effects did not affect the fit. Figure 4.16 shows the fit of the background. The rightmost Gaussian fit (labeled Gaussian Fit 1) is due to $B^+ \rightarrow J/\Psi K^{*+}$ events.

Secondly, parameters of the background fit obtained by Monte Carlo truth matching are fixed. The thereby described fit function is used as part of the input to describe the total B^+ mass distribution of the J/Ψ inclusive and data sample. Then the background curve is

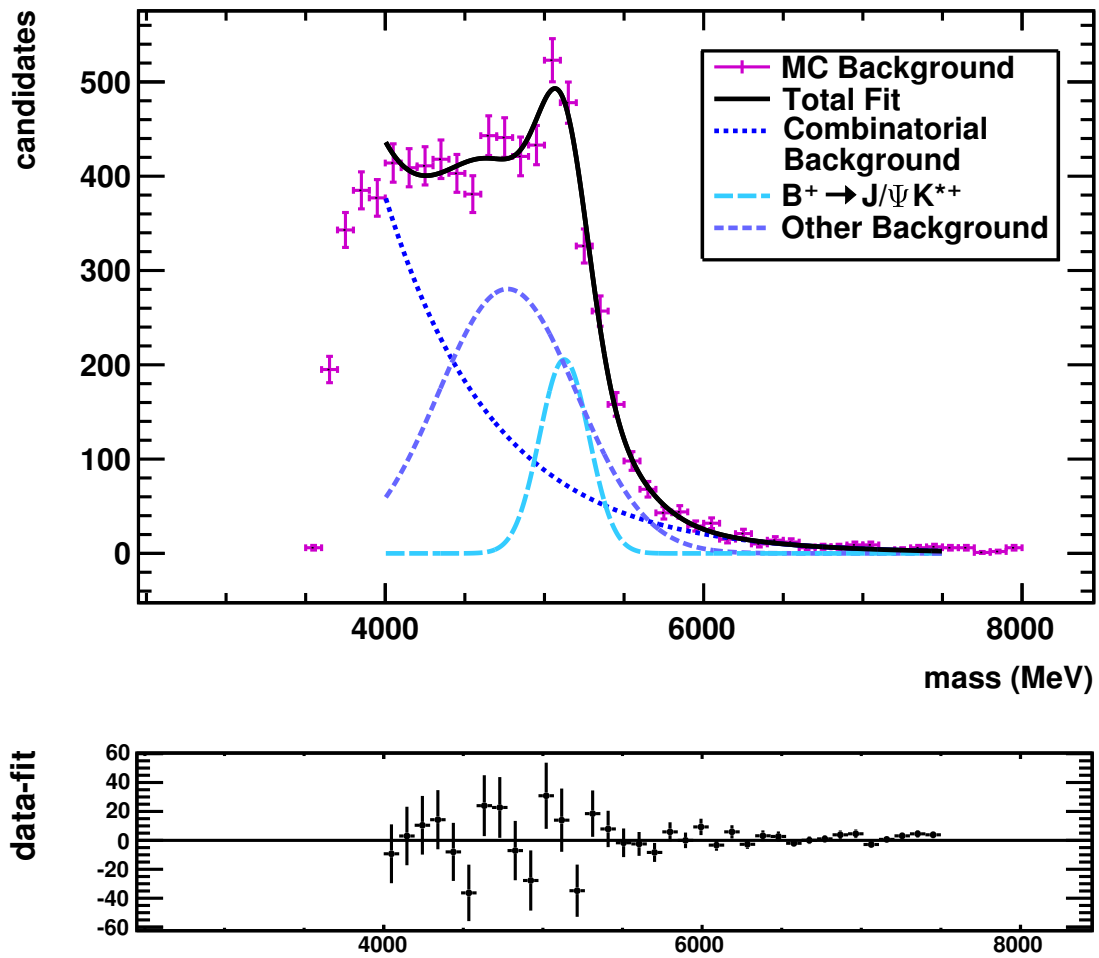


Figure 4.16: Top: The histogram of the background of the B^+ mass distribution is shown for a Monte Carlo J/Ψ inclusive sample. The functions the fit is composed of are separately drawn. Bottom: It is shown how good the fit represents the data points. Reasonable good agreement is reached.

combined with another Gaussian function which is adjusted by the fitting routine to describe the signal peak (fig. 4.17).

Mass Probability Distribution Function

The background fit obtained with a Monte Carlo sample is used to describe the background of other samples as well. To do so the fit has to be independent of the number of entries of the histogram. Therefore the fit has to be normalized. $B(m)/\mathcal{N}_B$ and $S(m)/\mathcal{N}_S$ in eqs. (4.7) and (4.8) are the normalized background function and the normalized signal function:

$$\frac{B(m)}{\mathcal{N}_B} = \frac{1}{I_B} \left[p_0 \exp [p_1 m] + p_2 \exp \left[-\frac{1}{2} \left(\frac{m - p_3}{p_4} \right)^2 \right] + p_5 \exp \left[-\frac{1}{2} \left(\frac{m - p_6}{p_7} \right)^2 \right] \right] \quad (4.7)$$

$$\frac{S(m)}{\mathcal{N}_S} = \frac{1}{\sqrt{2\pi p_9}} \exp \left[-\frac{1}{2} \left(\frac{m - p_8}{p_9} \right)^2 \right] \quad (4.8)$$

For the background function the normalization is performed by dividing the whole function through its integral I_B . The signal function on the other hand is a Gaussian function, which is normalized by definition. The fit parameters $p_0 - p_9$ describe the shape of the fitting curve.

To find the relative amount of signal candidates with respect to background candidates the probability distribution function, eq. (4.9) is arranged and implemented as a fitting routine.

$$PDF(m) = \left[\frac{B}{\mathcal{N}_B} (1 - f) + \frac{S}{\mathcal{N}_S} f \right] \quad (4.9)$$

Its input is:

- $B(m)/\mathcal{N}_B$, the normalized background function of the Monte Carlo sample ($p_0 - p_7$ are fixed)

The values determined by the fitting procedure are:

- $S(m)/\mathcal{N}_S$ by adjusting the parameters p_8 and p_9
- The scaling parameter f , which describes the relative amount of signal candidates with respect to all candidates. It is a number between 0 and 1. The bigger its value, the better the signal-to-background ratio.

As only normalized variables are input in eq. (4.9), it is independent of the number of entries of a histogram.

The portion f of signal candidates with respect to to all candidates in the distribution is called signal yield. To calculate the amount of signal events the signal yield has to be multiplied by all events in the histogram:

$$N_{Signal} = f \cdot N_{All\ Events} \quad (4.10)$$

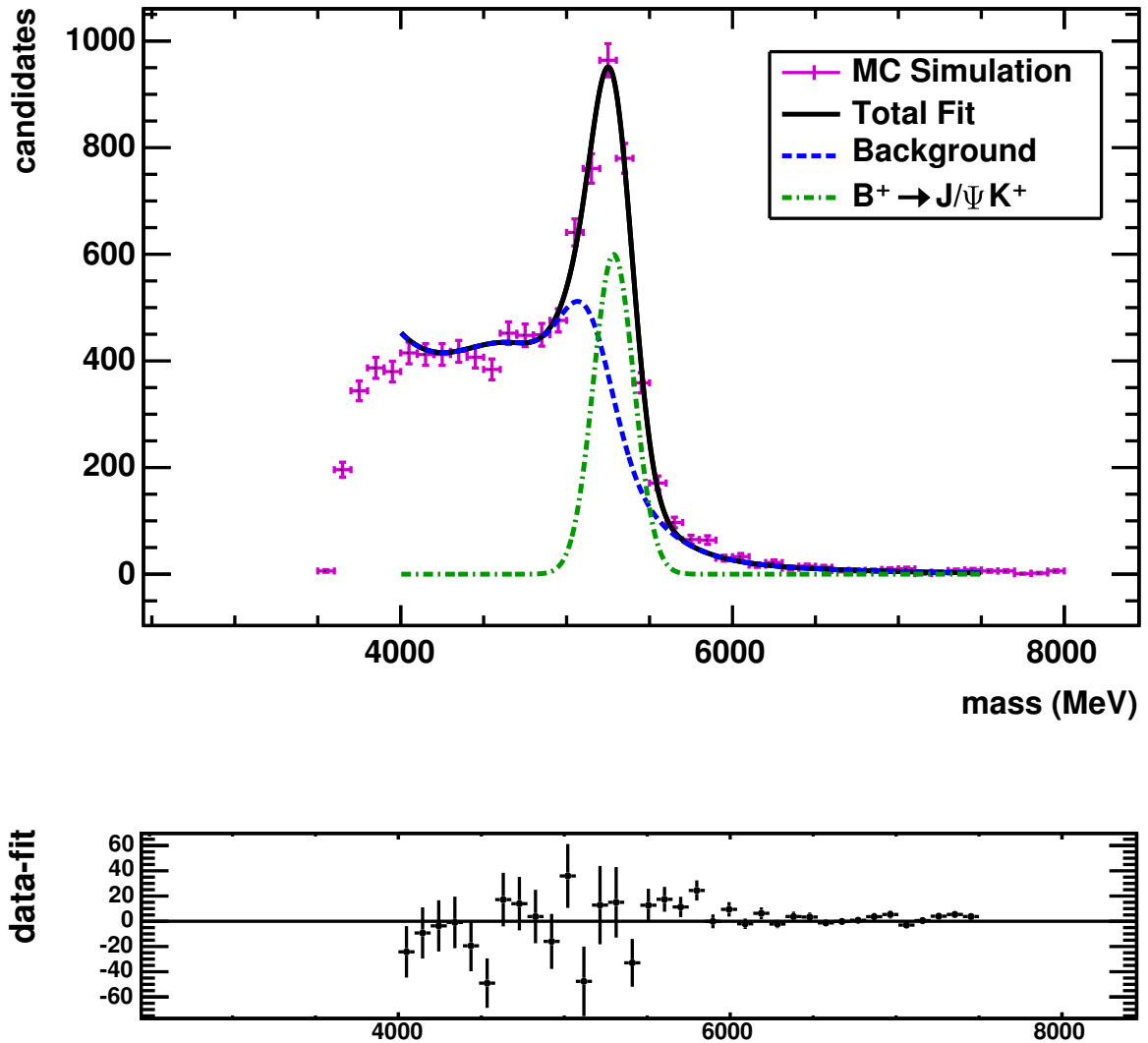


Figure 4.17: Top: Histogram of the distribution of the B^+ mass of a Monte Carlo sample and its fit. Shown are the fit of the whole distribution, the fit describing the background and the fit of the signal peak. Bottom: it is shown how good the fit represents the data points, i.e. how many entries the fit is off the right value.

4.7 Results of the Track Reconstruction Efficiency

The task to calculate the track reconstruction efficiency was performed with three analyses.

- **Simulation Sample; Tracks Within Detector Acceptance:** A pre-requisite for the first analysis is that only VELO stubs having an associated Monte Carlo particle are taken into account. However, the Monte Carlo particle is not required to be a kaon. Therefore, it is not Monte Carlo truth matched. The tracking efficiency is calculated defining probe legs as efficient in which the particle corresponding to a VELO stub is within the acceptance. The requirements for a particle to be within detector acceptance are that its angle is small enough to not leave the detector and that it has enough hits in the main tracking sub-detectors to be reconstructed. This means, it has to have a hit in three r and ϕ sensors of the Vertex Locator and one hit in a vertical and a tilted layer of all the tracking stations.
- **Simulation Sample; Search for Long Tracks:** The tracking efficiency is calculated by defining probe legs which have a corresponding long tracks as reconstructed. The procedure of finding a matching long track is described in section 4.6.1.
- **Data Sample; Search for Long Tracks:** The tracking efficiency is calculated in the same way as the preceding step, but instead of simulated data, data recorded by LHCb is taken.

Tracks can only be reconstructed, if the particles are within detector acceptance. Therefore, the first analysis gives an upper boundary for the reachable track reconstruction efficiency calculated with the presented method using partial reconstructed decays.

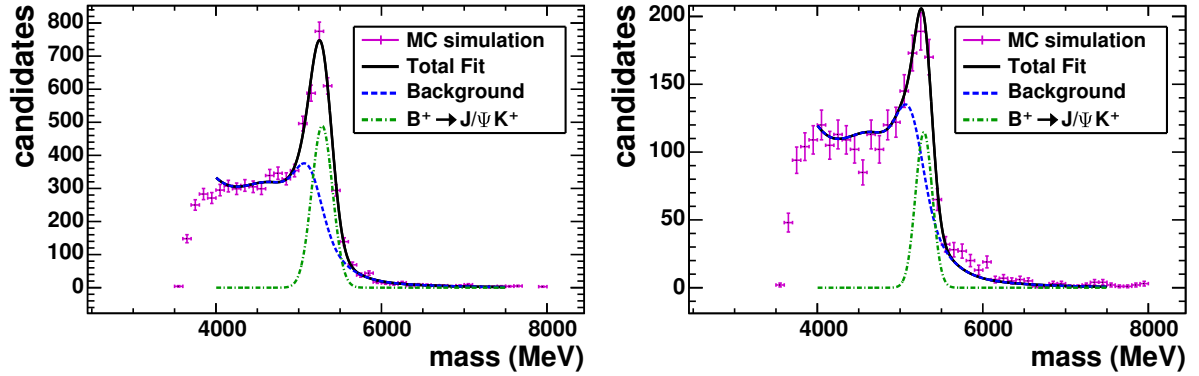
On the one hand the difference between the first and the second analysis gives insight to the performance of the track reconstruction algorithm. If the particle is within the acceptance of the detector, but not reconstructed as a long track, this can be due to inefficiencies of the reconstruction algorithms. On the other hand, the method of searching for a long track matching the VELO stub affects the difference between the first and the second analysis. With a higher probability of finding a matching long track, the track reconstruction efficiency increases.

The only difference between the second and the third analysis is that for the second one the input is simulated data, while for the third data taken in the LHCb experiment is used. Hence differences in the results are due to effects not described by simulations. These effects contain interactions with unknown detector material.

To calculate the track reconstruction efficiency two histograms are needed: One containing the candidates with reconstructed probe legs and one containing the candidates without reconstructed probe legs. With the amount of signal events derived as shown in section 4.6.2, the track reconstruction efficiency is calculated:

$$\epsilon = \frac{N_{\text{signal, reconstructed}}}{N_{\text{signal, reconstructed}} + N_{\text{signal, not reconstructed}}} \quad (4.11)$$

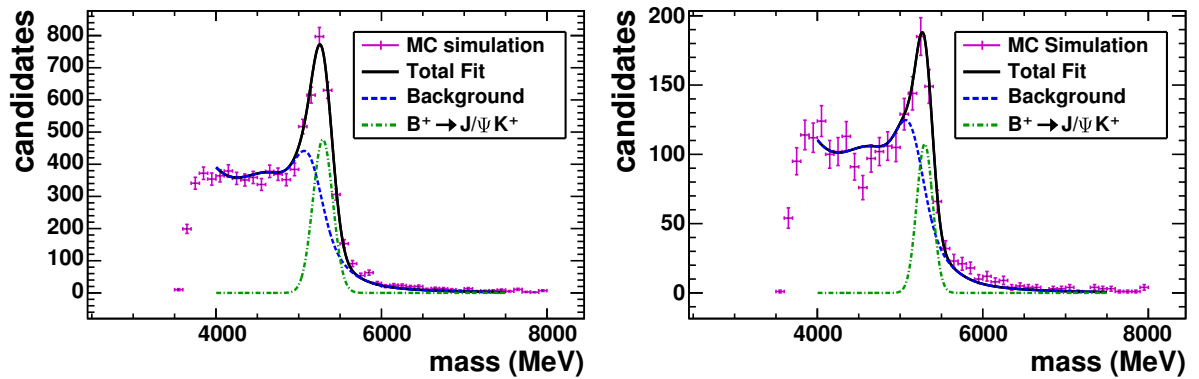
In figs. 4.18a to 4.20b the fitted histograms used for determining the amount of signal events is shown. In appendix A the fitting parameters are given for all distributions. In general, there are more events which are reconstructed than there are which are not reconstructed. Also the signal peak is smaller with respect to the background fit for the distributions in which the probe legs are not reconstructed.



(a) Monte Carlo particle associated to the VELO stubs within detector acceptance

(b) Monte Carlo particle associated to the VELO stub not within detector acceptance

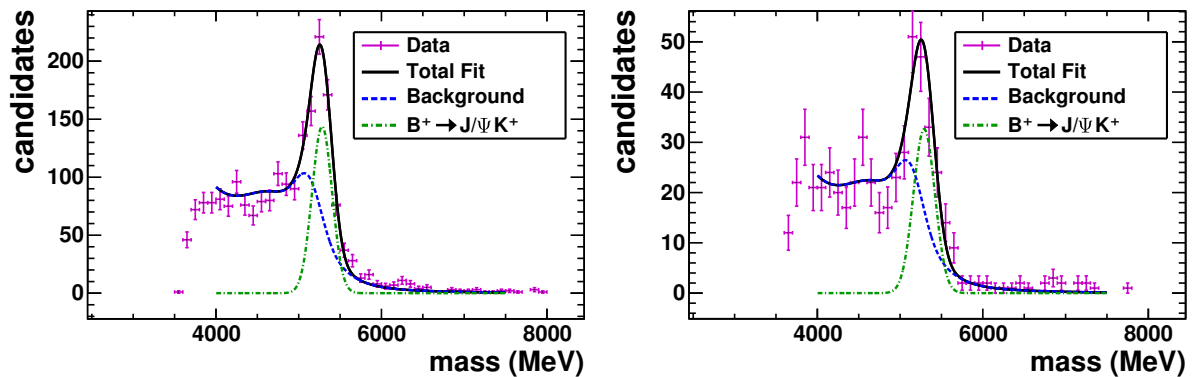
Figure 4.18: Fit of the invariant mass of the B^+ particle of partially reconstructed $B^+ \rightarrow J/\Psi K^+$ candidates obtained with simulated data.



(a) Matching long track found for the VELO stubs.

(b) No matching long track found for the VELO stubs.

Figure 4.19: Fit of the invariant mass of the B^+ particle of partially reconstructed $B^+ \rightarrow J/\Psi K^+$ candidates obtained with simulated data.



(a) Matching long track found for the VELO stubs.

(b) No matching long track found for the VELO stubs

Figure 4.20: Fit of the invariant mass of the B^+ particle of partially reconstructed $B^+ \rightarrow J/\Psi K^+$ candidates obtained with data taken by LHCb.

The track reconstruction efficiency obtained by calculation are:

- Monte Carlo simulation with VELO stubs within detector acceptance: $\epsilon = 84.1\% \pm 1.5\%$
- Monte Carlo simulation with long track matching the VELO stubs: $\epsilon = 84.5\% \pm 1.5\%$
- LHCb data with long track matching the VELO stubs: $\epsilon = 80.4\% \pm 2.5\%$

The given uncertainties are statistical uncertainties. They are calculated from the error of the signal yield f which is given by the fitting routine and the statistical uncertainties of the number of entries $N_{All\ Events}$. Once the analysis has been performed with more data, the value of the statistical uncertainties will decrease.

4.8 Discussion of Results

4.8.1 Error Calculation

Studies about the track reconstruction efficiency at LHCb have the goal to make measurements more accurate. The tracking efficiency is currently the largest systematic uncertainty on many measurements (chapter 1, [2]). The results of the New Physics analyses are at per mill-level. Regarding this it is important, that the errors on the result of the evaluated tracking efficiencies are below 1%.

With the available amount of data at the time of performing this analysis, the statistical uncertainties alone are bigger than 1%. Once more data is available, the numbers have to be re-evaluated and the systematical errors determined. The systematic uncertainties then have to be computed, taking into account the uncertainty due to the fit model, which is probably the biggest source of errors. Other sources of systematic uncertainties are the method of finding the matching long tracks and the values used for the cuts.

As the simulation sample is bigger, the statistical errors for those are smaller than for data taken by LHCb.

4.8.2 Comparison Monte Carlo- Data

The results for the analysis using simulated data and acceptance requirements, and the analysis using simulated data and long track matching are in good agreement with each other. Hence inefficiencies due to the tracking algorithms are negligible on Monte Carlo of this analysis. The procedure for long track matching works properly. Differences between simulated data and data taken by LHCb are assigned to unknown material effects not included in the Monte Carlo event generation.

4.8.3 Factors Reducing the Efficiency

Reasons for the track reconstruction efficiency being only little more than 80% have been investigated with the Monte Carlo J/Ψ inclusive sample. A B^+ particle of a $B^+ \rightarrow J/\Psi K^+$ decay cannot be reconstructed, if the kaon is not within detector acceptance, i.e. if the kaon either leaves the angular acceptance of the detector or if it does not fulfill the amount of hits required by the reconstruction algorithm. The contributing effects are:

- Kaons which interact with matter before they can be measured in all detector parts necessary for a long track reconstruction.
- Kaons which spontaneously decay in the detector before they can be measured in all detector parts necessary for long track reconstruction.
- Kaons which leave the angular detector acceptance before being reconstructed as a long track.
- Kaons which are not reconstructed due to inefficiencies of the track reconstruction algorithm.

Of the kaons which are not reconstructed, $93.8\% \pm 3.6\%$ decay before leaving enough hits to be reconstructed as a long track. This percentage contains kaons which interact with matter and kaons which decay in flight. Particle showers and decays with particles heavier than the kaon as decay products unambiguously indicate material interactions. Using this information,

detector part	# decays	decays per meter
Vertex Locator	868	789 ± 99
RICH1	429	390 ± 54
Trigger Tracker	409	584 ± 112
magnet	465	101 ± 7
T1	220	314 ± 66
T2	188	269 ± 58
T2	108	154 ± 37

Table 4.2: Amount of particle decays listed by the detector part and in which they decay. T1,T2 and T3 refer to the three tracking modules after the magnet.

a lower boundary for the percentage of kaons not reconstructed due to interactions with detector material is found to be 51%. About 43% of the kaons which are not reconstructed decay to lighter particles, mainly pions. These decays arise from material interactions or decays in flight.

The fact that about 6% of the kaons which cannot be reconstructed and did not decay within the detector indicates decays in which the kaon left the acceptance of the detector and decays which could not be reconstructed due to inefficiencies of the track reconstruction algorithm.

Figure 4.21 shows the z-position of the kaon decays. At the top, a sketch of the tracking part of the detector is drawn for reference, the histogram at the bottom shows how many particle decays take place at the which distance. It is clear that in sections where the particles have to traverse detector material, more decays happen due to interactions with matter. The two peaks just after 2 m and the three peaks between about 7.8 m and 10 m represent the interaction of particles with material of the tracking system. The effect that particles also decay in detector parts where they do not have to go through matter (e.g. inside the magnet) arises due to decays in flight. In table 4.2 the particle decays in the detector modules are summarized. The most decays per length happen in the Vertex Locator and the Trigger Tracker, because there is the biggest amount of kaons present which can decay.

In general, tracks which cannot be reconstructed are suppressed by applying appropriate cuts. However, in the here presented analysis additional cuts which have not been already applied would have affected the measurement too much to guarantee unbiased results.

4.8.4 Conclusion

Due to the fact that not enough data is available to reduce the statistical uncertainties to a value below the 1% level, the newly developed procedure to calculate the track reconstruction efficiency with the decay channel $B^+ \rightarrow J/\Psi K^+$ can not yet enhance physics analyses. Both the low value of the efficiency and the uncertainty of it are quantities which cannot be further improved within this method with the available amount of data. Therefore a new approach is made: Instead of the decay channel $B^+ \rightarrow J/\Psi K^+$ the high statistics decay channel $\Lambda \rightarrow p\pi^-$ is exploited.

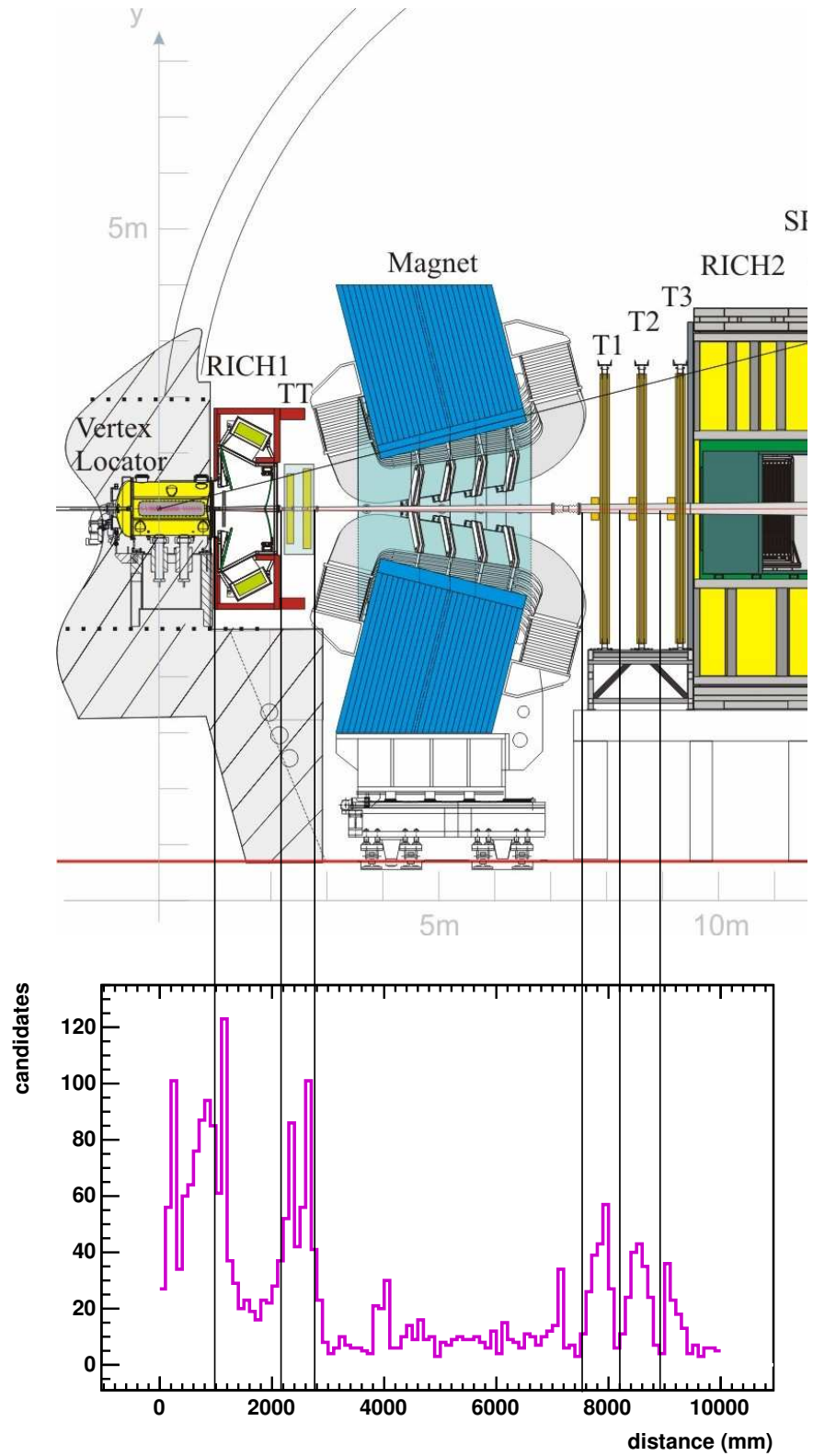


Figure 4.21: Top: Sketch of the first few meters of the LHCb detector. Bottom: Amount of particle decays at the respective distances.

Chapter 5

Measurement of the Tracking Efficiency on Data Using the Decay Channel $\Lambda \rightarrow p\pi^-$

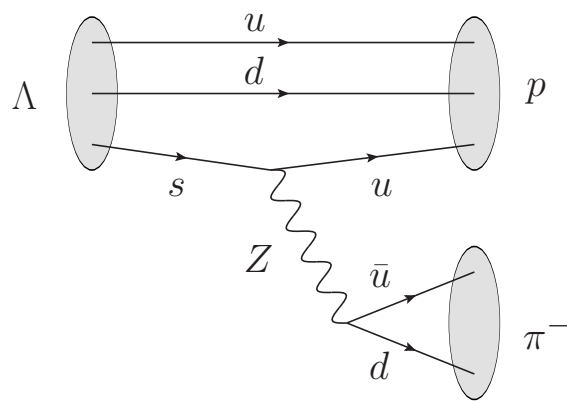
5.1 Introduction

In the last chapter, it was discussed that the accuracy of the track reconstruction efficiency needed for measuring effects below per mill level could not be reached using the $B^+ \rightarrow J/\Psi K^+$ sample. The problem arises due to too large statistical uncertainties. Hence the same procedure is tested with the high statistics decay channel $\Lambda \rightarrow p\pi^-$ (fig. 5.1) to reach the required precision. Additionally to the high production rate of Λ particles, another advantage of the $\Lambda \rightarrow p\pi^-$ decay is the high branching ratio of $\Lambda \rightarrow p\pi^-$ of $63.9\% \pm 0.5\%$ [17]. Hence most of the produced Λ particles decay into the final state investigated in this study.

LHCb is a dedicated B-physics experiment, therefore the primary aim is to find a way of retrieving the track reconstruction efficiency with tracks which cover the same phase space as B particles which are used in later analyses. The pion momentum distribution has a sufficient overlap with the J/Ψ momentum thus enabling reweighting of the $\Lambda \rightarrow p\pi^-$ distributions to fit the $B^+ \rightarrow J/\Psi K^+$ phase space. Due to the long life time of the Λ particle, it is more likely than the B particles to decay outside of the Vertex Locator. If this is the case, it cannot be properly reconstructed. However, there are enough Λ particles decaying within the Vertex Locator, that the available amount of $\Lambda \rightarrow p\pi^-$ candidates is still by orders of magnitude larger than the amount of $B^+ \rightarrow J/\Psi K^+$ candidates.

The workflow of the analysis using the $\Lambda \rightarrow p\pi^-$ sample is similar to the one exploiting the $B^+ \rightarrow J/\Psi K^+$ decays: At first the method is tested and developed with simulation data and later applied to data taken by the LHCb experiment.

Due to the limited amount of time, some issues of the study presented in this chapter remain subject to further improvements.

Figure 5.1: Feynman graph of a $\Lambda \rightarrow p\pi^-$ decay.

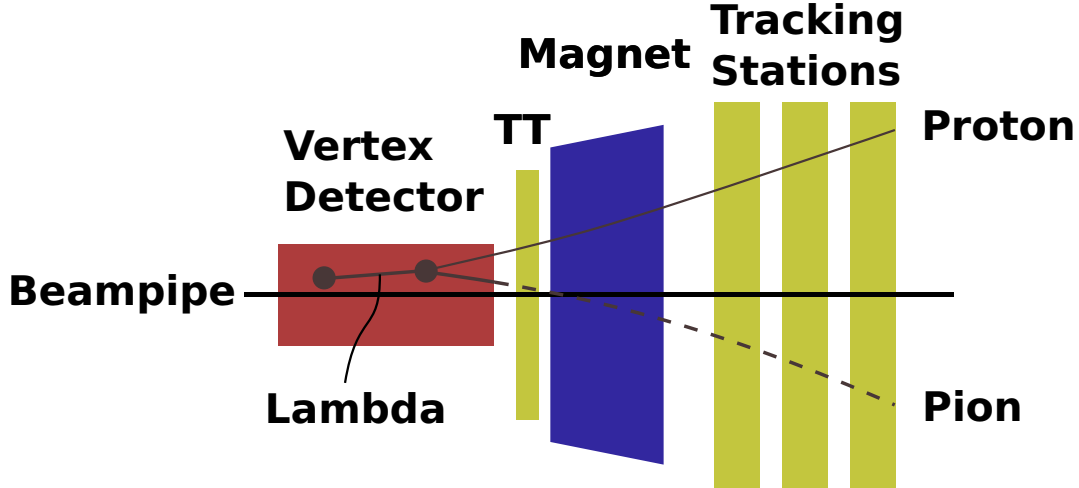


Figure 5.2: Sketch of the $\Lambda \rightarrow p\pi^-$ decay as it is recorded in the detector. The dashed pion line represents the detector information missing if only the VELO stub of the pion is taken into account.

5.2 Reconstruction of $\Lambda \rightarrow p\pi^-$ with Partial Reconstructed Pions

Analogous to the analysis using $B^+ \rightarrow J/\Psi K^+$ decays, a tag-and-probe method is applied to calculate the track reconstruction efficiency using $\Lambda \rightarrow p\pi^-$ decays. In this analysis, the probe leg is the VELO stub of the pion, the tag leg is the long track of the proton (fig. 5.2). The proton is the better choice for the tag leg, because it can be distinguished with high confidence from the large amount of pions present in the detector by particle identification.

The invariant mass of the Λ particle candidates provides a means of separating signal and background in the efficiency calculation. To derive it, at first it is necessary to find the VELO stub belonging to the $\Lambda \rightarrow p\pi^-$ decay. Equivalent to the method explained in section 4.3, the momentum of the particle represented by the VELO stub (in this case the pion candidate) is calculated. The calculation of the momentum is performed by maximizing the cosine between the combined momentum of the proton and the pion candidate:

$$\cos \alpha = \frac{\vec{e}_\Lambda \cdot (p_p \vec{e}_p + p_\pi \vec{e}_\pi)}{|\vec{e}_\Lambda| \cdot |p_p \vec{e}_p + p_\pi \vec{e}_\pi|} \quad (5.1)$$

As the cosine approaches 1, the combined momentum and the momentum of the Λ particle are parallel. Therefore momentum is conserved which is the condition for a VELO stub to belong to the pion of the $\Lambda \rightarrow p\pi^-$ candidate.

With the information about the momentum of the pion obtained with eq. (5.1), the decay is fully described. Via energy conservation, the invariant mass of the Λ particles is then calculated, forming a distribution for the Λ mass. To do so, a mass of 140 MeV and 938 MeV are assigned to the pion candidate and the proton, respectively.

5.3 Event Selection

For the analysis minimum bias events are used. This means, that the trigger requirements are minimal.

Before the particles are combined to form the data sample for the analysis, some pre-selection cuts are applied.

- Impact parameter χ^2 : Ensure that the particles stem from a displaced vertex instead of the primary vertex (table 5.1).
- Particle identification cut: Require that the tag track belongs to a proton.
- Vertex χ^2 : Restrain the proton and pion to stem from the same vertex.

Their values are listed in table 5.1.

For the final selection, two types of cuts are applied: The first type serves to reject combinatorial background, which is the major source of background. The second type enhances the probability, that the long track of the pion is within detector acceptance.

In the analysis with the Λ particles, less cuts are applied than for the analysis with the B^+ particle. For the analysis with B^+ particles, it is necessary to strongly reduce background to obtain a signal peak. Due to the large cross-section of the Λ particles, a clear signal peak of their invariant mass is already visible when applying only the pre-selection cuts.

Less variables exist which are suited for the application of cuts compared to the $B^+ \rightarrow J/\Psi K^+$ decay. The fact, that the secondary vertex of the $B^+ \rightarrow J/\Psi K^+$ decay is defined by three tracks (two muons and a kaon), makes the decay suited for more cuts, e.g. the cut on the distance between the J/Ψ vertex and the kaon track. As the secondary vertex of the $\Lambda \rightarrow p\pi^-$ is a two track vertex, this cut is not possible.

In the following, the selection cuts are described.

5.3.1 Candidate Selection Cuts

Lowest Λ χ^2

A candidate which is most probably an actual $\Lambda \rightarrow p\pi^-$ decay has to be found within the event. All other $\Lambda \rightarrow p\pi^-$ candidates of the event are considered as fake decays. The candidate with the lowest vertex χ^2 of the Λ particle is the most promising one and therefore selected. Thereby the probability that both tracks of the daughter candidates are daughters of the same mother is enhanced.

Cosine of Maximized Angle

To ensure that all particles combined to $\Lambda \rightarrow p\pi^-$ decays belong to the same decay, a cut on the maximized cosine between the combined momentum vector of the proton and the pion, and the momentum vector of the Λ particle is applied. If the cosine is equal to 1, the vectors are parallel, hence momentum is conserved and therefore a necessary condition for the particles to belong to the same decay is met.

Cut	Value
Pre-selection	
proton impact parameter χ^2	> 100
VELO stub impact parameter χ^2	> 100
proton particle identification	> 10
vertex χ^2	< 16
Final selection	
VELO stub momentum	> 2500 MeV
VELO stub pseudorapidity	> 3.2
cosine maximum angle	> 0.999998

Table 5.1: Cuts applied to $\Lambda \rightarrow p\pi^-$ samples.

5.3.2 Cuts to Enhance Reconstruction Probability

VELO Stub Pseudorapidity

Particles with a low pseudorapidity are more likely to be bent out of detector acceptance by the magnetic field. Therefore, a cut is applied to the pseudorapidity of the VELO stubs to enhance the probability that the matching long tracks are within detector acceptance.

VELO Stub Momentum

In section 5.2 it was described how to calculate the momentum of the pion. A cut is applied to this calculated value for the same reasons as mentioned above: Low momentum particles are likely to be bent out of the detector acceptance by the magnetic field.

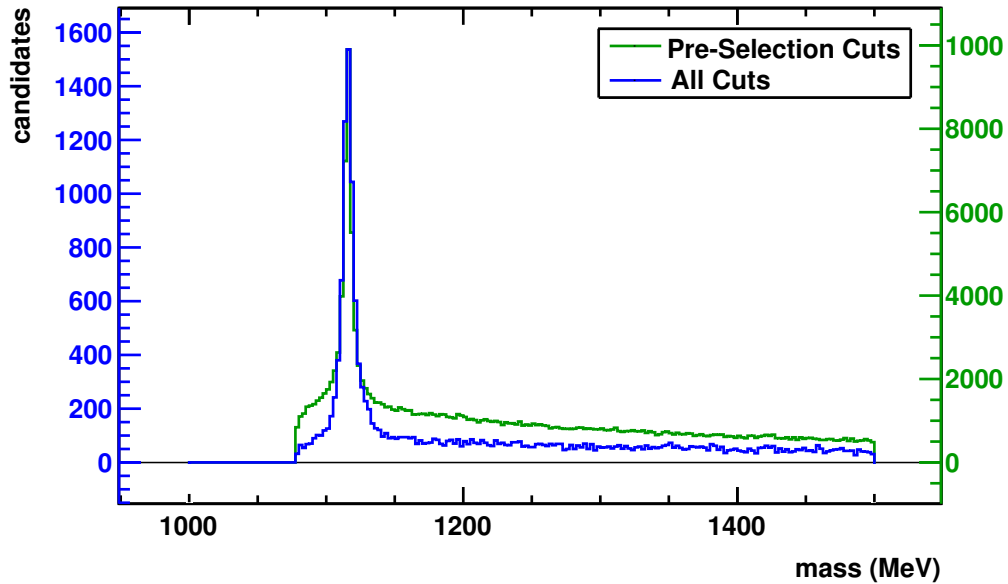


Figure 5.3: Plot of the mass of the Λ particles of the Monte Carlo $\Lambda \rightarrow p\pi^-$ sample. To obtain the blue histogram, all cuts mentioned in section 5.3 are applied, to obtain the green histogram only pre-selection cuts are applied.

5.4 Λ Mass Distribution

In section 5.2 it is explained how to calculate the mass distribution of the Λ particle. Therefore are the VELO stub of the pion and the long track of the proton taken into account. The method of using partially reconstructed decays to find the Λ particle's mass is applied to a Monte Carlo simulation sample of $\Lambda \rightarrow p\pi^-$ decays and on data from LHCb.

After applying only the pre-selection cuts (table 5.1) a clear mass peak rising above the background is already visible (fig. 5.3). This circumstance is explained by the large cross-section and the distinct particle identification of the Λ particles.

There is no other decay with a final state consisting of one proton and one pion with a similarly high branching ratio as $\Lambda \rightarrow p\pi^-$. Therefore, if these daughter particles are found it is very likely that they belong to a Λ decay. Hence if all particles are correctly identified there should be hardly any physical background.

5.4.1 Monte Carlo $\Lambda \rightarrow p\pi^-$ Sample

For Monte Carlo studies, a sample of about 430 000 events is used. With Monte Carlo truth matching, the peak of the $\Lambda \rightarrow p\pi^-$ particles is separated from background which is due to other decays (fig. 5.4). A double Gaussian curve with different mean values for each Gaussian proved to be the best fit to describe the signal distribution. The literature value of the Λ mass is 1115.683 ± 0.006 MeV [17]. The peak obtained with the combination of the momenta of the daughter particles with simulated data lies at about 1115 MeV. Therefore the method of calculating the invariant mass with partially reconstructed decays is suited for the determination of the Λ mass.

Figure 5.3 shows Λ particles found with the method using partially reconstructed decays. The smooth curve suggests that combinatorial background is the dominant source of back-

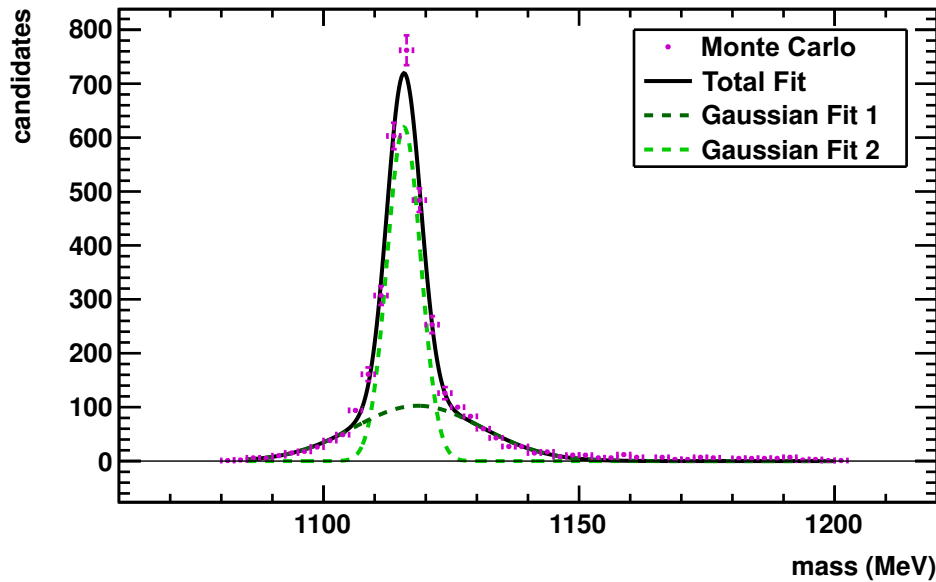


Figure 5.4: Plot of the invariant mass of Monte Carlo truth matched Λ particles obtained with the method of partially reconstructed decays; peak of the narrow fit at 1115.73 ± 0.09 MeV.

ground. For the blue histogram all of the the cuts discussed in section 5.3 are applied. By comparing it with the histogram obtained after applying the pre-selection cuts, it can be seen that background is reduced with respect to signal. On the left-hand side the mass distribution falls off. This is due to the kinematic threshold: A particle decaying into a proton (mass: 938 MeV) and a pion (mass: 140 MeV) can under no circumstances be lighter than the sum of the two, which is about 1078 MeV.

5.4.2 Data Sample

For the analysis using data from the LHCb, a sample of 23 million events is used. The method to evaluate the Λ mass exploiting simulated $\Lambda \rightarrow p\pi^-$ decays is applied in the same way to data using the same selection cuts (fig. 5.5).

The obtained mass distribution is similar to the results of the simulation sample. The background curve is smooth, however compared to the Monte Carlo sample, the signal-to-background ratio is smaller. This implies that there is more combinatoric background, hence there are more random tracks combined to form a $\Lambda \rightarrow p\pi^-$ candidate.

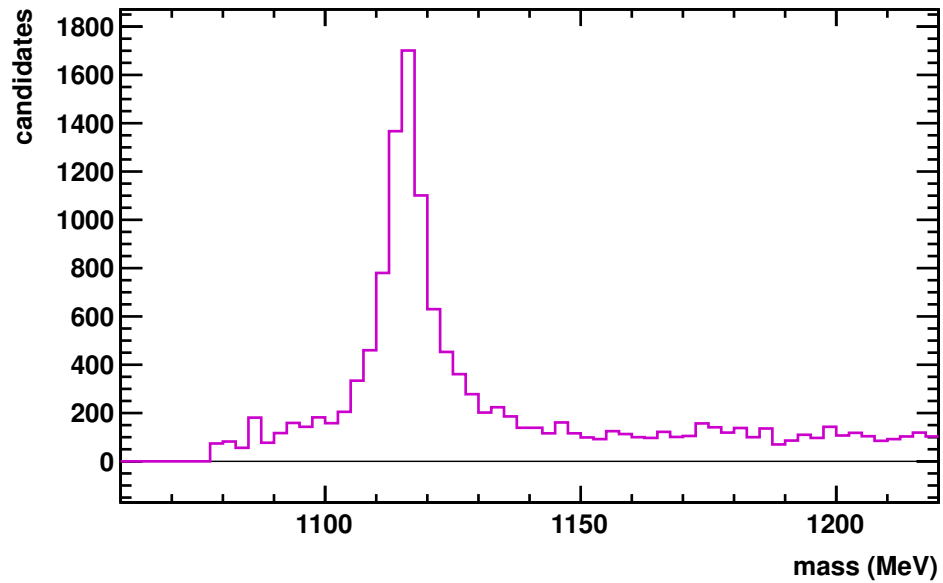


Figure 5.5: Plot of the mass distribution of the Λ particles obtained with the method of partially reconstructed decays using LHCb data.

5.5 Efficiency Calculation

The efficiency calculation using Λ decays is similar to the calculation exploiting $B^+ \rightarrow J/\Psi K^+$ data. However, as there is no physical background, the background curve does not have to be determined with simulated data first. The combinatorial background is derived from the sidebands. In the following paragraphs it is explained how to calculate the efficiency if the signal and background distribution can be fitted in one step, as it is the case for the $\Lambda \rightarrow p\pi^-$ sample.

5.5.1 Signal - Background Separation

As mentioned due to the kinematic threshold, there is a lower limit for the calculation of the Λ mass by combining a pion and a proton (fig. 5.6). The peak of the invariant mass of the Λ particle is just above this threshold.

As discussed in section 5.4.1, the signal curve is best described by a double-Gaussian curve with different mean values for each Gaussian. Due to the kinematic threshold only a range starting at 1090 MeV is fitted. Within this range the background is represented by an exponential curve. At the bottom of fig. 5.6, it is shown that the fit describes the mass distribution reasonably well.

Using data from the LHCb, the same fitting routine as for simulated data is applied (fig. 5.7). The kinematic threshold has a much more distinct shape in LHCb data than in simulation, but it is not within the fitting range. However, compared to the amount of background candidates which are described by the exponential decay, there is a low amount of candidates in this low mass regime.

The mathematical form of the fit is given in eqs. (5.2) and (5.3). $B(m)/\mathcal{N}_B$ denotes the normalized background curve, $S(m)/\mathcal{N}_S$ denotes the normalized signal curve.

$$\frac{B(m)}{\mathcal{N}_B} = \frac{1}{I_B} \cdot p_1 \exp [p_2 m] \quad (5.2)$$

$$\frac{S(m)}{\mathcal{N}_S} = \frac{1}{p_3 + p_6} \left[\frac{p_3}{\sqrt{2\pi}p_5} \exp \left[-\frac{1}{2} \left(\frac{m - p_4}{p_5} \right)^2 \right] + \frac{p_6}{\sqrt{2\pi}p_8} \exp \left[-\frac{1}{2} \left(\frac{m - p_7}{p_8} \right)^2 \right] \right] \quad (5.3)$$

The background function is normalized by dividing it by its integral I_B . The parameters p_3 and p_6 give the size of the Gaussian curves, therefore their sum defines the normalization factor \mathcal{N}_S of the signal function. In total, there are eight parameters ($p_1 - p_8$) to be found by the fitting routine.

The amount of signal events is then calculated according to eqs. (4.9) and (4.10).

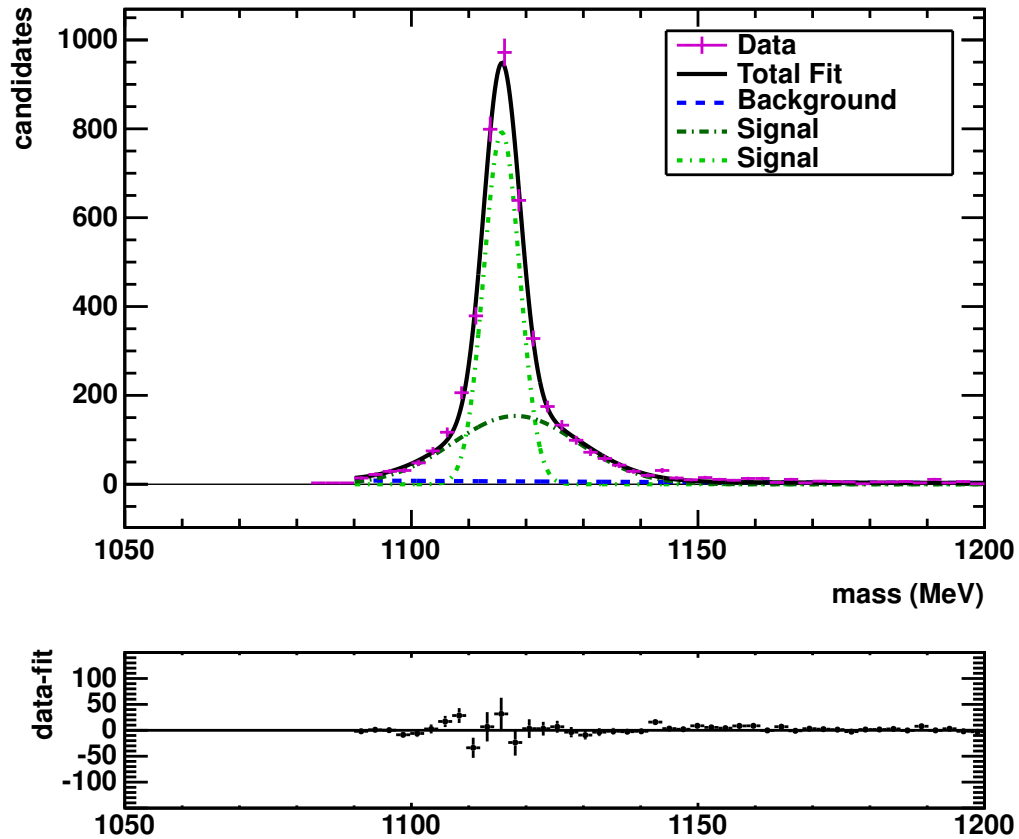


Figure 5.6: Top: Fit of the mass distribution of the Λ particles of a Monte Carlo sample. It is required that an associated Monte Carlo particle exists for every VELO stub. The combined fit (black) is put together of the double-Gaussian signal peak and the exponential background curve. Bottom: Goodness of the fit. Shown are the differences in the number of entries in the bin and the value of the fit curve at that point.

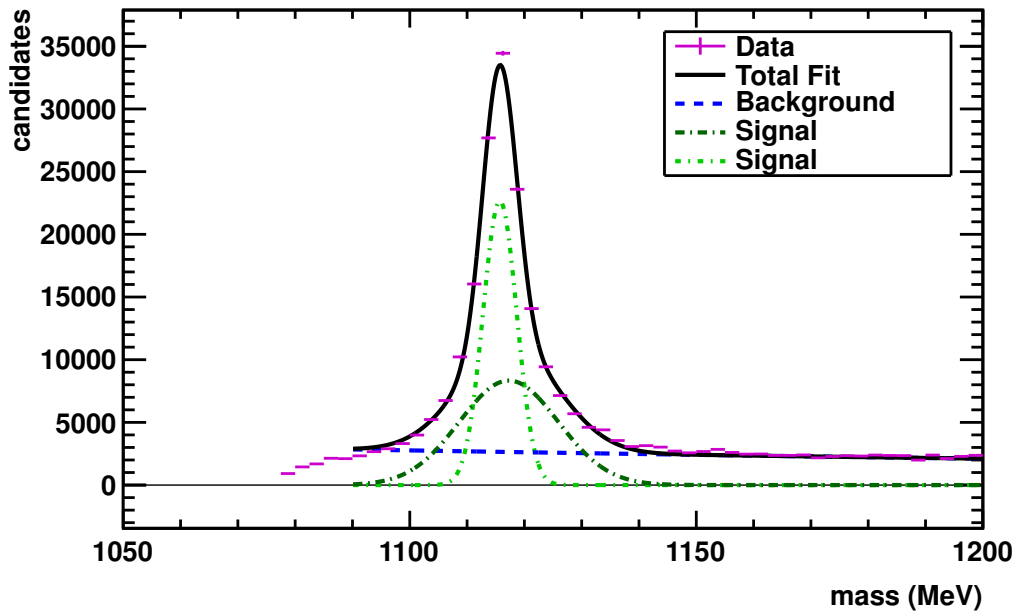


Figure 5.7: Fit of the mass distribution of the Λ particles of a data sample. The combined fit (black) is put together of the Gaussian signal peak and the exponential background curve.

5.6 Results and Discussion of the Track Reconstruction Efficiency

Three analyses for the track reconstruction efficiency have been carried out. These are the same as in the study using $B^+ \rightarrow J/\Psi K^+$ samples (section 4.7).

- Monte Carlo simulation data. Distinction whether tracks of the particles assigned to the VELO stubs are or are not within detector acceptance (section 4.6). For this approach, only VELO stubs having an associated Monte Carlo particle are taken into account. These are not required to be pions.
- Application of the developed method using Monte Carlo simulation data. A long tracks matching the VELO stubs is searched.
- Application of the developed method using data taken in the LHCb experiment. Also a long tracks matching the VELO stubs is searched.

To calculate the track reconstruction efficiency the Λ mass probability distribution is fitted both for decays in which the probe leg is considered as reconstructed and for decays in which the the probe leg is considered as not reconstructed. This is done for all three analyses (figs. 5.8 to 5.10). The fit parameters are listed in appendix A.

There are more candidates in detector acceptance than candidates not in detector acceptance. Analogous, the number of candidates with a matching long track is higher than the number without a matching long track. However, to make statements about the track reconstruction efficiency the signal-to-background ratio has to be taken into account. There is hardly any combinatorial background in the plots obtained with the Monte Carlo sample by requiring the Monte Carlo particles assigned to the VELO stubs to be within detector acceptance. For the analyses using matching long tracks, there is more background.

With the amount of signal events derived as shown in section 5.5.1, the track reconstruction efficiency is calculated:

$$\epsilon = \frac{N_{\text{signal, efficient}}}{N_{\text{signal, efficient}} + N_{\text{signal, not efficient}}} \quad (5.4)$$

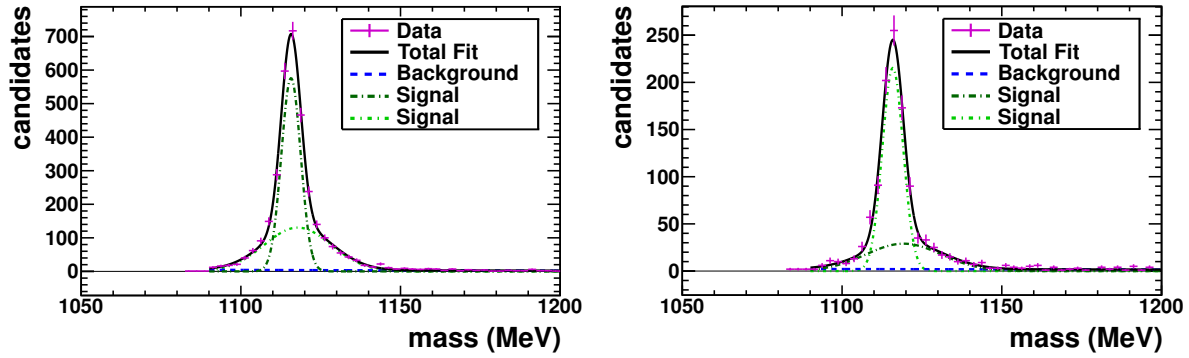
The obtained results are:

- Monte Carlo sample with VELO stubs in acceptance: $75.27\% \pm 0.40\%$
- Monte Carlo sample with VELO stubs matched to long tracks: $71.05\% \pm 0.37\%$
- Data sample with VELO stubs matched to long tracks: $59.21\% \pm 0.07\%$

Due to the fact that LHCb is a dedicated B-physics experiment, the tracking algorithms are optimized for the reconstruction of B particles. Therefore, the values of the track reconstruction efficiency of the Λ particles are lower than the values for the B particles.

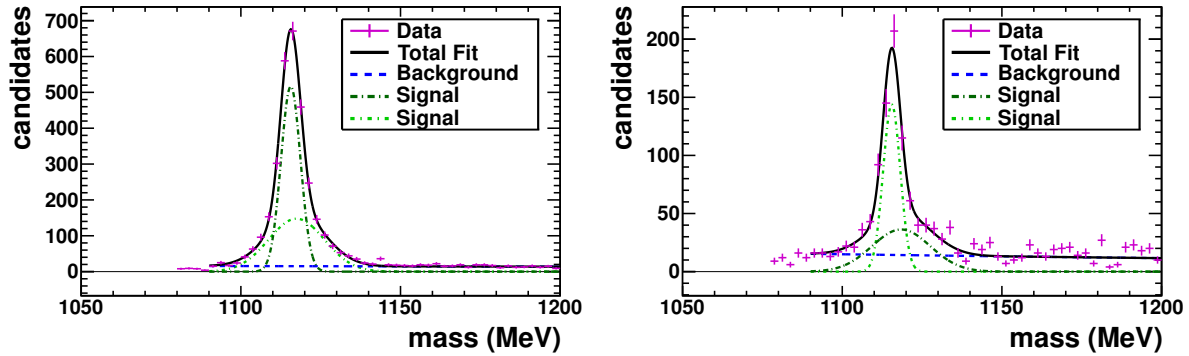
The fact that the efficiency of the analysis using a Monte Carlo sample searching for matching long tracks is lower than the efficiency of all the tracks within detector acceptance suggests inefficiencies of the procedure of finding a matching long track.

The difference between the result for Monte Carlo using long track matching and data suggests that there are effects, which are not yet fully understood. Further studies are needed to find explanations. There could be differences in the momentum and angular distributions,



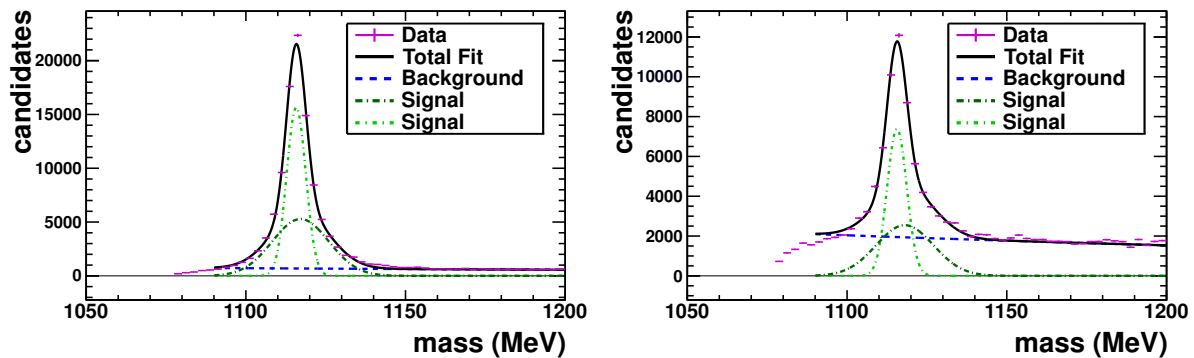
(a) Monte Carlo particle associated to the VELO stub within detector acceptance.

(b) Monte Carlo particle associated to the VELO stub not within detector acceptance.

Figure 5.8: Fit of the Λ mass obtained with simulated data.

(a) Matching long track found for the VELO stubs.

(b) No matching long track found for the VELO stubs.

Figure 5.9: Fit of the Λ mass obtained with simulated data.

(a) Matching long track found for the VELO stubs.

(b) No matching long track found for the VELO stubs

Figure 5.10: Fit of the Λ mass obtained with data taken in LHCb.

which would lead to the necessity of reweighting the samples to deal with data in the same momentum and angular regime.

The given uncertainties are statistical uncertainties. The small statistic uncertainties imply that the fit describes the data reasonably well. The calculation of the systematic uncertainties has to be performed once the missing adjustments summarized in section 5.6.1 are carried out.

5.6.1 Outlook

The future steps needed for the evaluation of the track reconstruction efficiency exploiting $\Lambda \rightarrow p\pi^-$ events contain the following:

- Further development has to be put into the the algorithm used for finding long tracks which match the VELO stubs.
- Investigate the momentum and pseudorapidity and reweight Monte Carlo if necessary.
- Once the preceding points have been put into the analysis, the systematic uncertainties have to be evaluated.
- To make the study compatible with B decays, investigate the phase space of the Λ decays and reweight according to the B phase space.

Chapter 6

Conclusion

The purpose of the presented analysis is to determine the influence of material interactions on the track reconstruction efficiency in a data-driven analysis.

A tag-and-probe is developed using $B^+ \rightarrow J/\Psi(\mu\mu)K^+$ decays. The kaon is hereby only reconstructed in the Vertex Locator and serves as probe for the efficiency measurement. The probe leg is considered as reconstructed if a matching long track is found. To statistically separate signal from the combinatorial and physical background the B^+ mass distribution is fitted.

The evaluated track reconstruction efficiency using simulated data is ($\sim 830\,000$ events):

$$\epsilon_{simulation} = 84.1\% \pm 1.5\%(\text{stat.}) \quad (6.1)$$

Using data taken in the LHCb experiment it is ($\sim 195\,000$ events):

$$\epsilon_{data} = 80.4\% \pm 2.5\%(\text{stat.}) \quad (6.2)$$

These findings are in reasonable good agreement with each other, which implies that the material effects are properly described by the simulation within the given uncertainties. Despite the limited statistics, the novel method is proven to work and will be repeated on a larger data set already taken by the LHCb experiment.

To apply the analysis to a larger data set, the method is performed with the high-statistics channel $\Lambda \rightarrow p\pi^-$. This analysis has the additional advantage of negligible physical background and the possibility to separately study positively and negatively charged tracks. The obtained statistical uncertainty is 0.07%, which is a very promising result. However, further studies are needed to evaluate possible systematic effects and to perform detailed comparisons of data with Monte Carlo simulations.

Appendix A

Fit Parameters

A.1 $B^+ \rightarrow J/\Psi K^+$

In the following tables the fit parameters chosen for calculating the track reconstruction efficiency using eqs. (4.7) to (4.9) are listed.

Parameter	Value	Error
p_0	128143	45567.5
p_1	-0.00145619	5.94069e-05
p_2	205.529	28.2295
p_3	5124.56	16.3257
p_4	155.054	25.2439
p_5	280.409	19.1544
p_6	4767.95	70.1349
p_6	434.024	39.0004

Table A.1: Fitting parameters for the background function. $\chi^2 = 43.8384$

Parameter	Value	Error
p_8	5283.11	5.39857
p_9	125.877	5.28809
f	0.242759	0.00942769

Table A.2: Monte Carlo in acceptance $\chi^2 = 35.6567$

Parameter	Value	Error
p_8	5288.21	12.3007
p_9	101.739	11.5854
f	0.144561	0.0150366

Table A.3: Monte Carlo not in acceptance $\chi^2 = 54.9194$

Parameter	Value	Error
p_8	5291.67	5.40102
p_9	120.271	5.60476
f	0.202598	0.00851658

Table A.4: Monte Carlo long tracks matched. $\chi^2 = 82.073$

Parameter	Value	Error
p_8	5297.64	10.9656
p_9	97.5022	10.9301
f	0.141225	0.0146771

Table A.5: Monte Carlo long tracks not matched. $\chi^2 = 47.6703$

Parameter	Value	Error
p_8	5282.6	9.34032
p_9	121.281	10.3211
f	0.247891	0.0176933

Table A.6: Data long tracks matched. $\chi^2 = 48.676$

Parameter	Value	Error
p_8	5290.84	25.7972
p_9	130.0	5.34594
f	0.238887	0.0309703

Table A.7: Data long tracks not matched. $\chi^2 = 28.7613$

A.2 $\Lambda \rightarrow p\pi^-$

In the following tables the fit parameters chosen for calculating the track reconstruction efficiency using eqs. (5.2) and (5.3) are listed.

Parameter	Value	Error
p_1	9797.6	47737.3
p_2	-0.00698537	0.00402136
p_3	4371.12	243.84
p_4	1115.71	0.102121
p_5	3.02897	0.140527
p_6	3428.05	217.723
p_7	1117.82	0.364968
p_8	10.4835	0.637476

Table A.8: Monte Carlo in acceptance. $\chi^2 = 53.461$

Parameter	Value	Error
p_1	64.9176	92.5264
p_2	-0.00308498	0.00109602
p_3	860.515	96.198
p_4	1119.27	0.866591
p_5	11.8367	0.955401
p_6	1765.47	108.609
p_7	1115.88	0.161413
p_8	3.27304	0.189097

Table A.9: Monte Carlo not in acceptance. $\chi^2 = 42.6651$

Parameter	Value	Error
p_1	52.6978	5.93135
p_2	-0.00111394	7.31979e-05
p_3	3952.03	319.202
p_4	1115.63	0.114887
p_5	3.05367	0.173876
p_6	3228.73	313.035
p_7	1117.42	0.429445
p_8	8.73145	0.545649

Table A.10: Monte Carlo long tracks matched. $\chi^2 = 181.89$

Parameter	Value	Error
p_1	244.716	83.3176
p_2	-0.00254203	0.000262623
p_3	826.885	118.745
p_4	1118.44	1.02316
p_5	9.10168	0.893711
p_6	968.223	112.333
p_7	1115.5	0.216528
p_8	2.68706	0.263779

Table A.11: Monte Carlo long tracks not matched. $\chi^2 = 395.548$

Parameter	Value	Error
p_1	9213.23	488.228
p_2	-0.00232811	4.06869e-05
p_3	117112	1954.03
p_4	1117.12	0.0666955
p_5	8.85379	0.106458
p_6	117531	2070.12
p_7	1115.78	0.0225562
p_8	2.99696	0.0387819

Table A.12: Data long tracks matched. $\chi^2 = 1012.24$

Parameter	Value	Error
p_1	46747.8	1373.26
p_2	-0.00284821	2.28703e-05
p_3	57145.1	1744.1
p_4	1118.07	0.203032
p_5	8.95533	0.202894
p_6	56826	1840.92
p_7	1115.61	0.0388259
p_8	3.07315	0.0665954

Table A.13: Data long tracks not matched. $\chi^2 = 459.96$

Appendix B

Derivation of Kaon Momentum

In the following it is shown, how to calculate the kaon momentum via maximization of the cosine between the B^+ momentum and the combined momentum between of the J/Ψ and the kaon momentum. The same derivation is applicable for the $\Lambda \rightarrow p\pi^-$ decay. For this, the B^+ is exchanged with the Λ , the J/Ψ with the p and the K with the π .

Special caution has to be taken with not mixing up the multiplication order. The “ \cdot ” sign represents the scalar product.

$$\begin{aligned}\cos \alpha &= \frac{\vec{e}_{B^+} \cdot (p_{J/\Psi} \vec{e}_{J/\Psi} + p_K \vec{e}_K)}{|\vec{e}_{B^+}| |p_{J/\Psi} \vec{e}_{J/\Psi} + p_K \vec{e}_K|} \\ &= \frac{\vec{e}_B \cdot (\vec{p}_{J/\Psi} + p_K \vec{e}_K)}{|\vec{p}_{J/\Psi} + p_K \vec{e}_K|} \\ \frac{d \cos \alpha}{dp_K} &= \frac{(\vec{e}_B \cdot \vec{e}_K) |\vec{p}_{J/\Psi} + p_K \vec{e}_K|}{|\vec{p}_{J/\Psi} + p_K \vec{e}_K|^2} \\ &\quad - \frac{\vec{e}_B \cdot (\vec{p}_{J/\Psi} + p_K \vec{e}_K)}{|\vec{p}_{J/\Psi} + p_K \vec{e}_K|^2} \frac{(\vec{p}_{J/\Psi} + p_K \vec{e}_K) \cdot \vec{e}_K}{|\vec{p}_{J/\Psi} + p_K \vec{e}_K|}\end{aligned}$$

Multiplication with the squared denominator leads to positive and negative terms.

$$\begin{aligned}0 &= \pm (\vec{e}_B \cdot \vec{e}_K) |\vec{p}_{J/\Psi} + p_K \vec{e}_K| \pm \\ &\quad \pm \vec{e}_B \cdot (\vec{p}_{J/\Psi} + p_K \vec{e}_K) \frac{(\vec{p}_{J/\Psi} + p_K \vec{e}_K) \cdot \vec{e}_K}{|\vec{p}_{J/\Psi} + p_K \vec{e}_K|} \\ &= \pm (\vec{e}_B \cdot \vec{e}_K) (\vec{p}_{J/\Psi} + p_K \vec{e}_K)^2 \\ &\quad \pm \vec{e}_B \cdot (\vec{p}_{J/\Psi} + p_K \vec{e}_K) (\vec{p}_{J/\Psi} + p_K \vec{e}_K) \cdot \vec{e}_K \\ &= \pm (\vec{e}_B \cdot \vec{e}_K) \left(\vec{p}_{J/\Psi}^2 + 2p_K \vec{p}_{J/\Psi} \vec{e}_K + p_K^2 \vec{e}_K^2 \right) \\ &\quad \pm \left[(\vec{e}_B \cdot \vec{p}_{J/\Psi} + p_K (\vec{e}_B \cdot \vec{e}_K)) (\vec{p}_{J/\Psi} \cdot \vec{e}_K + p_K \vec{e}_K \vec{e}_K) \right] \\ &= \pm \left[(\vec{e}_B \cdot \vec{e}_K) \vec{p}_{J/\Psi}^2 + 2p_K (\vec{e}_B \cdot \vec{e}_K) (\vec{p}_{J/\Psi} \cdot \vec{e}_K) + p_K^2 (\vec{e}_B \cdot \vec{e}_K) \right] \\ &\quad \pm \left[(\vec{e}_B \cdot \vec{e}_K) (\vec{p}_{J/\Psi} \cdot \vec{e}_K) + p_K (\vec{e}_B \cdot \vec{e}_K) (\vec{p}_{J/\Psi} \cdot \vec{e}_K) + \vec{e}_B \cdot \vec{p}_{J/\Psi} p_K + p_K^2 (\vec{e}_B \cdot \vec{e}_K) \right]\end{aligned}$$

Case distinction leads to three different results. Two evolve from the case in which either both terms are positive or both are negative.

Case 1:

$$\begin{aligned}
 0 &= (\vec{e}_B \cdot \vec{e}_K) \vec{p}_{J/\Psi}^2 + 3p_K (\vec{e}_B \cdot \vec{e}_K) (\vec{p}_{J/\Psi} \cdot \vec{e}_K) + 2p_K^2 (\vec{e}_B \cdot \vec{e}_K) \\
 &\quad + (\vec{e}_B \cdot \vec{p}_{J/\Psi}) (\vec{p}_{J/\Psi} \cdot \vec{e}_K) + p_K \vec{e}_B \cdot \vec{p}_{J/\Psi} \\
 &= 2(\vec{e}_B \cdot \vec{e}_K) p_K^2 + (3(\vec{e}_B \cdot \vec{e}_K) (\vec{p}_{J/\Psi} \cdot \vec{e}_K) + \vec{e}_B \cdot \vec{p}_{J/\Psi}) p_K \\
 &\quad + (\vec{e}_B \cdot \vec{e}_K) \vec{p}_{J/\Psi}^2 + (\vec{e}_B \cdot \vec{p}_{J/\Psi}) (\vec{p}_{J/\Psi} \cdot \vec{e}_K)
 \end{aligned}$$

Solving the quadratic equation in p_K :

$$p_{K1,2} = - \frac{U \pm \sqrt{U^2 - 8(\vec{e}_B \cdot \vec{e}_K) \left[(\vec{e}_B \cdot \vec{e}_K) \vec{p}_{J/\Psi}^2 + (\vec{e}_B \cdot \vec{p}_{J/\Psi}) (\vec{p}_{J/\Psi} \cdot \vec{e}_K) \right]}}{4(\vec{e}_B \cdot \vec{e}_K)}$$

Where

$$U = [3(\vec{e}_B \cdot \vec{e}_K) (\vec{p}_{J/\Psi} \cdot \vec{e}_K) + (\vec{e}_B \cdot \vec{p}_{J/\Psi})]$$

The third answer arises from the second case, in which one term is negative and one is positive.

Case 2:

$$p_{K3} = - \frac{(\vec{e}_B \cdot \vec{e}_K) \vec{p}_{J/\Psi}^2 - (\vec{e}_B \cdot \vec{p}_{J/\Psi}) (\vec{p}_{J/\Psi} \cdot \vec{e}_K)}{(\vec{p}_{J/\Psi} \cdot \vec{e}_K) (\vec{e}_B \cdot \vec{e}_K) - \vec{e}_B \cdot \vec{p}_{J/\Psi}}$$

Bibliography

- [1] Sebastian Wandernoth. Measurement of the $B_s^0 - \bar{B}_s^0$ mixing frequency and calibration of the same side tagger at lhcb, 2009. iii, 13
- [2] Andreas Jaeger, Paul Seyfert, Michel De Cian, Jeroen van Tilburg, and Stephanie Hansmann-Menzemer. Measurement of the track finding efficiency. Technical Report LHCb-PUB-2011-025. CERN-LHCb-PUB-2011-025, CERN, Geneva, Apr 2012. 1, 18, 20, 43
- [3] The ALICE Collaboration. The alice experiment at the cern lhc. *Journal of Instrumentation*, 3(08):S08002, 2008. 2
- [4] The ATLAS Collaboration. The atlas experiment at the cern large hadron collider. *Journal of Instrumentation*, 3(08):S08003, 2008. 2
- [5] The CMS Collaboration. The cms experiment at the cern lhc. *Journal of Instrumentation*, 3(08):S08004, 2008. 2
- [6] Lyndon R Evans and Philip Bryant. Lhc machine. *J. Instrum.*, 3:S08001. 164 p, 2008. This report is an abridged version of the LHC Design Report (CERN-2004-003). 3
- [7] The LHCb Collaboration. The lhcb detector at the lhc. *Journal of Instrumentation*, 3(08):S08005, 2008. 3, 4, 5, 6, 7, 9, 10, 15, 16
- [8] The LHCb Collaboration. *LHCb : Technical Proposal*. Tech. Proposal. CERN, Geneva, 1998. 5
- [9] Olaf Behrendt. The lhcb vertex locator. *Nucl. Instrum. Methods Phys. Res., A*, 598(1):61–63, 2009. 4
- [10] P R et al. Barbosa-Marinho. *LHCb VELO (VERTeX LOcator): Technical Design Report*. Technical Design Report LHCb. CERN, Geneva, 2001. 4
- [11] Eduardo Picatoste Olloqui. Lhcb preshower(ps) and scintillating pad detector (spd): commissioning, calibration, and monitoring. *J. Phys.: Conf. Ser.*, 160:012046. 8 p, 2009. 8, 9
- [12] Valentin Niess and the LHCb Collaboration. Commissioning of the lhcb preshower detector with cosmic rays and first lhc collisions. *Journal of Physics: Conference Series*, 293(1):012060, 2011. 9
- [13] S. Amato and others. *LHCb calorimeters: Technical Design Report*. Technical Design Report LHCb. CERN, Geneva, 2000. 9

-
- [14] R. Antunes-Nobrega and others. *LHCb trigger system: Technical Design Report*. Technical Design Report LHCb. CERN, Geneva, 2003. revised version number 1 submitted on 2003-09-24 12:12:22. 9
- [15] R Aaij, J Albrecht, F Alessio, S Amato, E Aslanides, et al. The LHCb Trigger and its Performance, 2012. 11
- [16] URL: http://en.wikipedia.org/wiki/Standard_Model. 11
- [17] J. Beringer and others (Particle Data Group). Review of particle physics. *Physical Review D*, 86:010001+, 2012. 12, 46, 51
- [18] Manuel Tobias Schiller. *Track reconstruction and prompt $Ks0$ production at the LHCb Experiment*. PhD thesis, Ruperto-Carola University of Heidelberg, Germany, 2011. 12, 15, 17
- [19] The LHCb Collaboration. Roadmap for selected key measurements of lhcb. 2009. 12
- [20] URL:<https://twiki.cern.ch/twiki/bin/view/LHCb/LHCbTrackingStrategies>. 17

Index

- antiparticle, **11**
- B-Physics, **2, 8**
- Cherenkov radiation, **8**
- CP violation, **12**
- DaVinci, **18**
- Downstream tracks, **16**
- electromagnetic calorimeter, **3, 9**
- forward tracking, **17**
- hadronic calorimeter, **3, 9**
- High Level Trigger, **10**
- hits, **14**
- HLT, *see* High Level Trigger
- Inner Tracker, **6**
- instantaneous luminosity, **3**
- LHC, **2**
- LHCb, **3**
- Long tracks, **16**
- Monte Carlo particles, **17**
- Monte Carlo truth matched, **25**
- muon identification system, **3**
- Muon Stations, **9**
- Muon System, **9**
- Outer Tracker, **7**
- PreShower Detector, **9**
- pseudorapidity, **3**
- reconstructed, **18**
- reconstructed particles, **17, 18**
- reconstructible, **18**
- RICH, *see* Ring Imaging Cherenkov Detectors
- Ring Imaging Cherenkov Detector, **3, 8**
- Scintillator Pad Detector, **9**
- SPD/PS, **9**
- Standard Model, **11**
- T tracks, **16**
- track matching, **17**
- tracking, **6**
- tracking stations, **3, 6**
- tracks, **14**
- trigger, **8, 9**
- Trigger Tracker, **6, 6**
- TT, *see* Trigger Tracker
- Upstream tracks, **16**
- VELO stub, **22**
- VELO tracks, **15**
- Vertex Locator, **3, 4**